Hydrodynamic fields induced by the shock response of a fluid-filled submerged cylindrical shell containing a rigid co-axial core

S. Iakovlev [a,*], J. Gaudet [a], G. Dooley [b], B. MacDonald [c]

[a] *Department of Engineering Mathematics and Internetworking, Dalhousie University, Halifax, Nova Scotia, Canada B3J 2X4*
[b] *Department of Mechanical Engineering, Dalhousie University, Halifax, Nova Scotia, Canada B3J 2X4*
[c] *IMP Group Ltd, 565 Barnes Road, Waverly, Nova Scotia, Canada B2T 1K3*

ARTICLE INFO

ABSTRACT

The hydrodynamic fields induced by the response to an external shock wave of a system consisting of a submerged fluid-filled cylindrical shell and a rigid cylindrical co-axial core are considered. The primary focus of the study is on the complexity brought into the interaction by the presence of the core, and on the analysis of the multitude of the respective shock wave propagation and reflection phenomena. It is shown that when the core is small, its overall impact on the interaction is insignificant, although the hydrodynamic patterns observed exhibit some interesting features even in that case. As the radius of the core increases, its effect on the interaction becomes more and more pronounced, with the internal wave pattern eventually becoming dramatically different from what is observed in the no-core case. As a part of this investigation, the exact reasons for the significant reduction of the tensile stress reported for a larger core in earlier studies are identified. Finally, when the core becomes sufficiently large to dominate the internal volume, the fluid between the shell and the core starts to behave as a fluid layer, and exhibits some properties similar to those of a waveguide.

© 2010 Elsevier Ltd. All rights reserved.

1. Introduction

The present work addresses the interaction between a fluid-filled submerged circular cylindrical shell with a rigid co-axial core placed inside it and an external shock wave, and focuses on the fluid dynamics aspect of the interaction. Analyzing the shock response of such a system is of interest for a number of reasons. First, systems of co-axial cylinders with fluid in between are common in naval architecture and nuclear engineering (e.g. [1] and references therein), ballast tanks being one example. Second, analyzing the interaction in this, rather simple from the structural point of view, case will allow for a better understanding of more complex systems, for example those incorporating several co-axial shells, a promising avenue for introducing safer and more efficient industrial structures.

The study is also intended to complement the first author's earlier investigation of the structural dynamics of the shell in the present system [2] where the focus was almost exclusively on the dynamics of the stress–strain state. Although most of the important structural effects observed were relatively easily explained in that work, the analysis of the fluid dynamics of the interaction was 'implicit': the actual hydrodynamic fields were not simulated, and the conclusions made were based on general hypothesizing about what was happening in the fluids based on the structural dynamics, without seeing the images of the pressure patterns.

---

* Corresponding author.
  E-mail address: serguei.iakovlev@dal.ca (S. Iakovlev).

Nomenclature[1]

c_f	sound speed in the fluid, $\hat{c}_f = 1$
c_s	sound speed in the shell material, $\hat{c}_s = c_s c_f^{-1}$
E_s	Young's modulus, $\hat{E}_s = E_s \rho_f^{-1} c_f^{-2}$
h_0	thickness of the shell, $\hat{h}_0 = h_0 r_0^{-1}$
I_n	modified Bessel function of the first kind of order n
J_n	Bessel function of the first kind of order n
K_n	modified Bessel function of the second kind of order n
p	total pressure in the fluid, $\hat{p} = p \rho_f^{-1} c_f^{-2}$
p_α	peak incident pressure, $\hat{p}_\alpha = p_\alpha \rho_f^{-1} c_f^{-2}$
p_0	incident pressure, $\hat{p}_0 = p_0 \rho_f^{-1} c_f^{-2}$
p_d	diffraction pressure, $\hat{p}_d = p_d \rho_f^{-1} c_f^{-2}$
p_r^i	internal radiation pressure, $\hat{p}_r^i = p_r^i \rho_f^{-1} c_f^{-2}$
p_r^e	external radiation pressure, $\hat{p}_r^e = p_r^e \rho_f^{-1} c_f^{-2}$
r	radial coordinate of the polar coordinate system, $r = \varrho r_0^{-1}$
r_0	radius of the shell, $\hat{r}_0 = 1$
R_0	radial distance to the source of the incident wave, $\hat{R}_0 = R_0 r_0^{-1}$
S_R	incident shock wave stand-off, $\hat{S}_R = S_R r_0^{-1}$
t	time, $t = \tau c_f r_0^{-1}$
v^*	transverse displacement of the middle surface of the shell, $v = v^* r_0^{-1}$
w^*	normal displacement of the middle surface of the shell, $w = w^* r_0^{-1}$
Y_n	Bessel function of the second kind of order n
θ	angular coordinate of the polar coordinate system
λ	exponential decay rate, $\hat{\lambda} = \lambda c_f r_0^{-1}$
v	Poisson's ratio
ξ_n^c	internal response functions
ξ_n^e	external response functions
ρ_f	density of the fluid, $\hat{\rho}_f = 1$
ρ_s	density of the shell material, $\hat{\rho}_s = \rho_s \rho_f^{-1}$
ϱ	radial coordinate of the polar coordinate system, $r = \varrho r_0^{-1}$
τ	time, $t = \tau c_f r_0^{-1}$
ϕ	fluid velocity potential in the fluid, $\hat{\phi} = \phi c_f^{-1} r_0^{-1}$
ϕ_0	fluid velocity potential in the incident wave, $\hat{\phi}_0 = \phi_0 c_f^{-1} r_0^{-1}$
ϕ_e	fluid velocity potential in the external fluid, $\hat{\phi}_e = \phi_e c_f^{-1} r_0^{-1}$
ϕ_d	fluid velocity potential in the diffracted wave, $\hat{\phi}_d = \phi_d c_f^{-1} r_0^{-1}$
ϕ_i	fluid velocity potential in the internal fluid, $\hat{\phi}_i = \phi_i c_f^{-1} r_0^{-1}$
ϕ_r^e	fluid velocity potential in the external radiated wave, $\hat{\phi}_r^e = \phi_r^e c_f^{-1} r_0^{-1}$
ϕ_r^i	fluid velocity potential in the internal radiated wave, $\hat{\phi}_r^i = \phi_r^i c_f^{-1} r_0^{-1}$

Such an 'implicit' approach worked fairly well, and the big picture of the structural dynamics was quite clear. However, even though it was obvious that the stress reduction was due to the changes of the internal pressure pattern caused by the presence of the core, the exact reduction mechanism was not clear. In particular, it was not well understood why the radius of the core had to be increased to approximately half of that of the shell for one to start noticing a significant decrease in the maximum tensile stress at the point diametrically opposite of the point of impact. It obviously had to do with how the internal wave pattern was modified by the core, but it was difficult, if at all possible, to give any specific explanation without actually seeing the respective images of the hydrodynamic field.

The uncertainty mentioned is not surprising considering the phenomenological complexity of the fluid dynamics inside a fluid-filled shock-responding shell (which was only reported, in the present context, after the results for the structural dynamics were published, [3,4]). The primary, and to a lesser degree secondary, Mach stems, as well as the focusing of the internal pressure wave after its reflection from the inner shell surface all contribute to the complexity of the internal hydrodynamic field. The main drawback, therefore, was the difficulty with making reliable predictions about the fluid dynamics aspect of the interaction without actual visualizing the hydrodynamic fields. The objective of the present work is to fill that gap.

As for the literature published on the topic, circular cylindrical shells with additional structural elements have been studied in the context of fluid–structure interaction for several decades, as have been systems of cylindrical shells. Specifically, [5] is an earlier example of an analytical study of a system of two concentric cylindrical shells where the focus was on the structural dynamics; the hydrodynamic fields were not visualized. Being one of the simplest, yet most practically important multi-shell systems, this design has been investigated extensively over the years, and some rather advanced studies taking into account such complex phenomena as shock-induced cavitation are available for it, for example [6].

More complex setups incorporating shells and/or rigid-wall confinements with internal elements were studied as well. For example, Jialing and Hongli [7] considered two rigid cylinders placed inside a rigid-wall channel conveying a shock wave, and studied the scattering patterns that developed around the cylinders as the shock wave moved over them. Both experimental and numerical images were presented, and relatively late stages of the diffraction from both cylinders (especially the one located higher upstream) and channel walls was addressed. Although not directly relevant to the present study, those results are quite helpful in understanding some general effects observed for non-stationary scattering by confined cylinders.

---

[1] $(*)_n \sin n\theta$ and $(*)_n \cos n\theta$ denote the harmonics of $(*)$. Unless stated otherwise, capitalized symbols denote the Laplace transforms of the corresponding functions. Other symbols are defined in the text.

Structural enhancements using spherical structures appear to be addressed more extensively than those employing cylindrical structures. For example, Kubenko and Dzuba [8] considered a pulsating spherical structure inside a fluid-filled circular cylindrical shell surrounded by an elastic medium, but only addressed harmonic motion (a number of references to earlier works dealing with internal spherical elements can be found in that work as well). Olsson [9] considered an external sphere in the proximity of a circular cylinder, and studied acoustic scattering by such a system, but only addressed stationary insonification. Again, even though not directly relevant to the present work, these studies are certainly useful for general understanding of the dynamics of multi-element systems. We note that the focus on spherical structures added to the primary cylindrical one is not a coincidence, but rather a reflection of the practitioner's needs as far as ocean engineering and naval architecture are concerned.

Advanced combinations of multiple cylindrical structures interacting with fluid have received attention as well, and usually the respective studies were aimed at modeling specific industrial systems that had a very specific geometry. For example, Oakley et al. [10] considered a system of three cylinders placed inside a larger cylindrical confinement, and studied the response of such a system to an external shock wave. The study was intended for the analysis of the shock response of certain structural components of a nuclear reactor. The focus was on the propagation of shock waves in the internal fluid, and their reflection off the inner cylinders. The structural effect of the primary or reflected waves on the confining surface was not addressed.

Considerably more structurally advanced system was addressed in a recent study by Sigrist et al. [11] who considered a system incorporating a large number of cylindrical structures equally spaced throughout the fluid domain occupying the space confined by two much larger co-axial cylindrical shells (again, with application to nuclear power generation). The fluid–structure interaction was modeled exactly, i.e., every internal structure was considered as a distinct entity interacting with surrounding fluid and experiencing the effects of the walls of the confinement and neighboring structures. The latter approach was a considerably more realistic representation of the actual interaction than the so-called homogenization technique where the geometrical complexity is not modeled exactly but is accounted for by means of introducing a 'homogenized' fluid domain. Such an approach is very efficient sometimes but often it does not allow for capturing the more subtle but important details of fluid–structure interaction; further discussion of the matter can be found in [11].

Finally, we mention that there are a number of studies where a thin fluid layer between two cylindrical structures is addressed. This is a so-called squeeze-film, with a heat exchanger and its support plate being one example of the relevant practical system, and squeeze film dampers in rotating machinery being another (e.g. [12] and references therein). However, the physics of such interaction is very different from the one addressed here, and the results of the squeeze-film studies are of little use as far as the objectives of the present work are concerned.

Thus, summarizing this literature review, it appears that the hydrodynamic fields inside an elastic shell responding to an external shock wave and containing an internal rigid cylindrical structure have not yet been investigated. Moreover, it also seems that the fluid dynamics of such interaction has not been explicitly put in the context of the respective structural dynamics either. The present study aims at addressing both of these issues.

2. Mathematical formulation

We consider a circular cylindrical shell containing an absolutely rigid co-axial core, Fig. 1. The radius of the shell is r_0, its thickness is h_0, and the radius of the core is a, $a < r_0$. We assume that $h_0/r_0 \ll 1$, and also that the deflections of the shell surface are small compared to its thickness, hence the linear theory of thin shells applies (we note that a detailed discussion of the difference between the shock-induced hydrodynamic fields computed using the linear theory of thin shells and a complete elastic model can be found in [13]). The density, Poisson's ratio, and Young's modulus of the shell
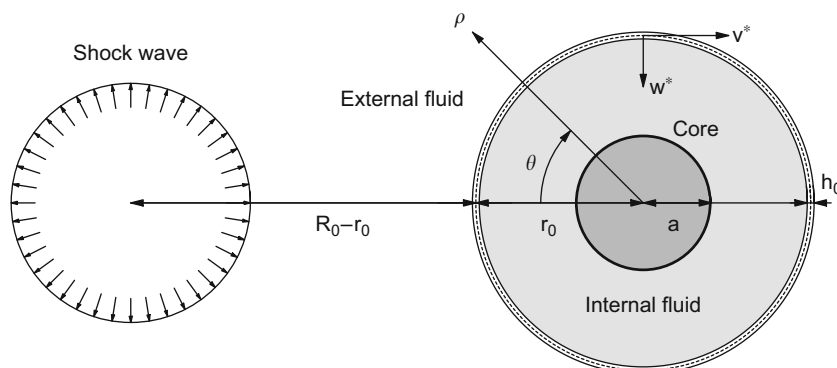

Fig. 1. Schematic of the problem.

material are ρ_s, v, and E_s, respectively, and the sound speed in the shell is $c_s = \sqrt{E_s/\{\rho_s(1-v^2)\}}$. The transverse and normal displacements of the middle surface of the shell are v^* and w^*, respectively. The shell is submerged into a fluid with the density ρ_f and sound speed c_f, and the space between the shell and the core is filled with the same fluid. The fluid is assumed to be irrotational, inviscid, and linearly compressible. Although considering two different fluids does not result in a significantly more complex solution, the focus of the present work is on the complexity brought in by the presence of the core, and not that due to the differences in the fluid properties. Thus, we only consider the case of identical fluids inside and outside, leaving the general scenario of different fluids for future investigation. The polar coordinates (ϱ, θ) based on the axis of the shell are employed.

We assume that the shell is subjected to an external shock wave the potential ϕ_0 in which is given by

$$\phi_0 = -\frac{\lambda p_\alpha S_R}{\rho_e R^*}\, e^{-(\tau-c_e^{-1}(R^*-S_R))\lambda^{-1}}\, H(\tau-c_e^{-1}(R^*-S_R)), \tag{1}$$

where

$$R^* = \sqrt{R_0^2 + \varrho^2 - 2R_0\varrho\cos\theta}, \tag{2}$$

p_α is the pressure in the front of the wave when it first contacts the shell, λ is the rate of exponential decay, $S_R = R_0 - r_0$ is the distance between the source and the shell (the shock wave stand-off), and H is the Heaviside unit step function. This shock wave is 'cylindrical' in a sense that it does not have the longitudinal variation of pressure associated with it, and considering such a wave is equivalent to addressing a 2D simplification of the problem where the middle cross-section of a spherical shock wave is extended indefinitely in both directions. There are certain relatively minor issues arising when such a wave is considered (see [14] for a detailed discussion), but the benefits of using it significantly outweigh the drawbacks. Specifically, the simplified 2D model captures the most important features of the interaction very well [4], and allows one to obtain a very realistic approximation to what would be seen in the middle cross-section of a shell subjected to a 3D incident wave. At the same time, the computational time and mathematical complexity are reduced dramatically.

The fluid is governed by the wave equations,

$$\nabla^2 \phi_i = \frac{1}{c_f^2}\frac{\partial^2 \phi_i}{\partial \tau^2}, \tag{3}$$

and

$$\nabla^2 \phi_e = \frac{1}{c_f^2}\frac{\partial^2 \phi_e}{\partial \tau^2}, \tag{4}$$

where ϕ_i and ϕ_e are the internal and external fluid velocity potentials, respectively, and τ is time.

We assume that the Love–Kirchhoff hypothesis holds true, hence the shell equations in displacements are (e.g. [15]; note that here we assume the normal displacement to be positive inward, whereas in [15] it is assumed to be positive outward; as a result, some of the terms appear in the equations below with different signs than are found in [15])

$$\frac{1}{r_0^2}\frac{\partial^2 v^*}{\partial \theta^2} - \frac{1}{r_0^2}\frac{\partial w^*}{\partial \theta} + k_0^2\left(\frac{1}{r_0^2}\frac{\partial^3 w^*}{\partial \theta^3} + \frac{1}{r_0^2}\frac{\partial^2 v^*}{\partial \theta^2}\right) = \frac{1}{c_s^2}\frac{\partial^2 v^*}{\partial \tau^2}, \tag{5}$$

$$\frac{1}{r_0^2}w^* - \frac{1}{r_0^2}\frac{\partial v^*}{\partial \theta} + k_0^2\left(\frac{1}{r_0^2}\frac{\partial^4 w^*}{\partial \theta^4} + \frac{1}{r_0^2}\frac{\partial^3 v^*}{\partial \theta^3}\right) = \chi p|_{\varrho = r_0} - \frac{1}{c_s^2}\frac{\partial^2 w^*}{\partial \tau^2}, \tag{6}$$

where $k_0^2 = h_0^2/(12r_0^2)$, $\chi = 1/(h_0\rho_s c_s^2)$, and p is the total acoustic pressure. The pressure p is comprised several components,

$$p = p_0 + p_d + p_r^e - p_r^i, \tag{7}$$

where p_0 is the incident pressure, p_d is the diffraction pressure, p_r^i is the internal radiation pressure, and p_{re} is the external radiation pressure.

There are a number of boundary conditions including the dynamic conditions on the interface,

$$\left.\frac{\partial \phi_r^i}{\partial \varrho}\right|_{\varrho = r_0} = -\frac{\partial w^*}{\partial \tau}, \tag{8}$$

$$\left.\frac{\partial \phi_r^e}{\partial \varrho}\right|_{\varrho = r_0} = -\frac{\partial w^*}{\partial \tau}, \tag{9}$$

the 'no-flow' conditions on the shell surface

$$\left.\frac{\partial\phi_d}{\partial\varrho}\right|_{\varrho=r_0} = -\left.\frac{\partial\phi_0}{\partial\varrho}\right|_{\varrho=r_0} \tag{10}$$

and the surface of the core

$$\left.\frac{\partial\phi_r^i}{\partial\varrho}\right|_{\varrho=a} = 0, \tag{11}$$

the decay conditions at the infinity

$$\phi_d\longrightarrow0 \quad\text{and}\quad \phi_r^e\longrightarrow0 \quad\text{when } \varrho\to\infty, \tag{12}$$

and the periodicity conditions θ-wise. The initial conditions are assumed to be zero.

We consider a dimensionless formulation of the problem, and normalize all variables to r_0, c_e, and ρ_f. It allows for a better applicability of the results to systems with considerably different dimensions, as well as makes the numerical values of the time variable more convenient to deal with. A 'hat' is normally used to distinguish a dimensionless variable from its dimensional counterpart, with the exception of the time $t = \tau c_e r_0^{-1}$, the radial coordinate $r = \varrho r_0^{-1}$, and the displacements, $w = w^* r_0^{-1}$ and $v = v^* r_0^{-1}$.

3. Fluid dynamics

Applying the Laplace transform to the wave equations (3) and (4) written in cylindrical coordinates, we have

$$\frac{\partial^2\hat{\Phi}}{\partial r^2} + \frac{1}{r}\frac{\partial\hat{\Phi}}{\partial r} + \frac{1}{r^2}\frac{\partial^2\hat{\Phi}}{\partial\theta^2} - s^2\hat{\Phi} = 0, \tag{13}$$

where $\hat{\Phi}$ stands for the Laplace transforms of both $\hat{\phi}_i$ and $\hat{\phi}_e$, and s is the transform variable. Then, we separate the spatial variables to obtain the general solution of (13) as

$$\hat{\Phi} = \{F_n K_n(rs) + G_n I_n(rs)\}\cos n\theta, \quad n = 0, 1, \ldots, \tag{14}$$

where I_n and K_n are the modified Bessel functions of the first and second kind of order n, respectively, and F_n and G_n are arbitrary functions of s.

We now assume the matching series expansions for the normal displacement of the shell surface and normal incident velocity at the interface,

$$w = \sum_{n=0}^{\infty} w_n(t)\cos n\theta \tag{15}$$

and

$$\left.\frac{\partial\hat{\phi}_0}{\partial r}\right|_{r=1} = \sum_{n=0}^{\infty} b_n(t)\cos n\theta, \tag{16}$$

respectively. After imposing the boundary conditions, the Laplace transforms of the harmonics of the potential components are obtained as

$$\hat{\Phi}_n^d(r,\theta,s) = B_n(s)\,\Xi_n^e(r,\,s)\cos n\theta, \tag{17}$$

$$\hat{\Phi}_n^{r,e}(r,\theta,s) = sW_n(s)\,\Xi_n^e(r,\,s)\cos n\theta \tag{18}$$

and

$$\hat{\Phi}_n^{r,i}(r,\theta,s) = -sW_n(s)\,\Xi_n^c(r,s)\,\cos n\theta, \tag{19}$$

where ξ_n^e and ξ_n^c are the response functions of the problem with the Laplace transforms Ξ_n^e and Ξ_n^c, respectively, given by

$$\Xi_n^e(r,s) = -\frac{K_n(rs)}{sK_n'(s)} \tag{20}$$

and

$$\Xi_n^c(a,r,s) = \frac{I_n'(as)\,K_n(rs) - K_n'(as)\,I_n(rs)}{s(K_n'(s)\,I_n'(as) - I_n'(s)\,K_n'(as))}, \tag{21}$$

and B_n and W_n are the Laplace transforms of b_n and w_n, respectively.

The response functions represent the response of the fluid to the radiation and scattering by the shell, and only depend on the geometry of the structure, not its physical properties or those of the fluids.

The expressions for the harmonics of the pressure are then easily obtained,

$$\hat{p}_n^d = -\frac{1}{\sqrt{r}} b_n(t) - \int_0^t b_n(\eta) \frac{d\xi_n^e}{d\eta}(r, t-\eta) \, d\eta, \tag{22}$$

$$\hat{p}_n^{r,e} = -\int_0^t \frac{d^2 w_n(\eta)}{d\eta^2} \xi_n^e(r, t-\eta) \, d\eta \tag{23}$$

and

$$\hat{p}_n^{r,i} = \int_0^t \frac{d^2 w_n(\eta)}{d\eta^2} \xi_n^c(r, t-\eta) \, d\eta, \tag{24}$$

and the components of the total pressure are expressed in a series form as

$$p_d = \sum_{n=0}^{\infty} p_n^d \cos n\theta, \quad p_r^e = \sum_{n=0}^{\infty} p_n^{r,e} \cos n\theta \quad \text{and} \quad p_r^i = \sum_{n=0}^{\infty} p_n^{r,i} \cos n\theta. \tag{25}$$

The problem has therefore been reduced to the computation of the response functions ξ_n^e and ξ_n^c. Once they are known, simulating the hydrodynamic field in and around the structure becomes a routine, although at times quite tedious, task.

The external response functions ξ_n^e have been addressed in detail in [16], and are not discussed here. The 'surface' version (i.e., $r=1$) of the internal response functions ξ_n^c was addressed in [2], where a numerical algorithm was used for the inversion of (21). Although numerical inversion was suitable for the rather limited amount of computations that the 'surface' version required, a more efficient approach is needed to simulate the entire hydrodynamic field inside the shell. Such an approach has been developed (see Appendix), and the functions ξ_n^c have been computed.

4. Structural dynamics

We expand the displacements into the following series:

$$v = \sum_{n=0}^{\infty} v_n \sin n\theta \tag{26}$$

and

$$w = \sum_{n=0}^{\infty} w_n \cos n\theta, \tag{27}$$

and rewrite the shell equations (5) and (6) in terms of the displacement harmonics $v_n \sin n\theta$ and $w_n \cos n\theta$. This results in an infinite set of integro-differential system for each pair of v_n and w_n,

$$\gamma^2 \frac{d^2 v_n}{dt^2} + c_n^{11} v_n + c_n^{12} w_n = 0, \tag{28}$$

$$\gamma^2 \frac{d^2 w_n}{dt^2} + c_n^{21} v_n + c_n^{22} w_n = \hat{\chi} \left\{ \hat{p}_n^0 + \hat{p}_n^d - \int_0^t \frac{d^2 w_n(\eta)}{d\eta^2} \xi_n^e(r, t-\eta) d\eta + \int_0^t \frac{d^2 w_n(\eta)}{d\eta^2} \xi_n^c(r, t-\eta) d\eta \right\} \bigg|_{r=1}, \tag{29}$$

where $c_n^{11} = n^2 + k_0^2 n^2$, $c_n^{12} = c_n^{21} = -n - k_0^2 n^3$, $c_{mn}^{22} = 1 + k_0^2 n^4$, $\hat{\chi} = (r_0 \rho_f c_f^2)/(h_0 \rho_s c_s^2)$, and $\gamma = \hat{c}_s^{-1}$.

The initial conditions for v_n, w_n, and their first derivatives are zero.

Although it is possible to obtain an analytical solution of the system (28) and (29) using the Laplace transform, a numerical approach based on a finite-difference approximation was shown [3] to be far more efficient (at least than the Laplace-transform-based approach tested when the work reported in [3] was in progress; we note here that in a similar shell-shock interaction context [17], an alternative approach was successfully used to solve a coupled problem where instead of a finite-difference methodology, the Laplace transform was employed to obtain the functions of interest in the frequency domain, and then a specific numerical technique was used to carry out the inverse transform). A simple explicit finite-difference scheme is used here where the integrals are approximated using the trapezoidal rule, and central differences are used to approximate the second derivatives,

$$v_n^{i+1} = 2v_n^i - v_n^{i-1} - h^2 \gamma^{-2} \{c_n^{11} v_n^i + c_n^{12} w_n^i\}, \tag{30}$$

$$w_n^{i+1} = 2w_n^i - w_n^{i-1} + \Omega_h \{\delta_h(p_n^i - h J_n^i - h I_n^i) - c_n^{21} v_n^i - c_n^{22} w_n^i\}, \tag{31}$$

where $\delta_h = \rho_f \gamma^2 r_0 (\rho_s h_0)^{-1}$, $\Omega_h = 2h^2 \rho_f \{\delta_h h (\rho_f + \rho_s \gamma^2) + 2\gamma^2 \rho_f\}^{-1}$, h is the time step,

$$J_n^i = \sum_{j=1}^{i-1} \{w_n^{j+1} - 2w_n^j + w_n^{j-1}\} h^{-2} \xi_{n,e}^{i-j}, \tag{32}$$

$$I_n^i = \frac{\rho_s c_s}{\rho_f c_f} \sum_{j=1}^{i-1} \{w_n^{j+1} - 2w_n^j + w_n^{j-1}\} h^{-2} \xi_{n,c}^{i-j}, \tag{33}$$

$\xi_{n,e}^i$ and $\xi_{n,c}^i$ stand for the i-node values of $\xi_n^e(1,t)$ and $\xi_n^c(1,t)$, respectively, and p_n^i stands for the i-node value of $\hat{p}_n^0 + \hat{p}_n^d$.

The convergence of a nearly identical scheme was analyzed in [18] for a submerged fluid-filled shell without a core, and it was found that the time step size of 0.001 guarantees the convergence of the scheme for all scenarios of interest. Similar convergence analysis was also carried out for an empty shell [16], and the step size of 0.001 was found sufficient as well. There are no reasons to believe that the situation is significantly different in the present case, and the step size of 0.001 was adopted in this study.

Furthermore, the number of harmonics necessary to simulate the interaction sufficiently accurately needs to be estimated as well (by being sufficiently accurate we mean not only being within the acceptable 5 percent error margin, but also ensuring that the simulated hydrodynamic fields will not have any apparent non-physical features; the latter often imposes much stricter requirements on the accuracy of the numerical procedure, e.g. [16]). Such an estimate was carried out for the external interaction in [16], and it was found that 300 harmonics are needed to realistically visualized the external hydrodynamic field (with the diffraction pressure being more demanding than the radiation one), and 150 harmonics are required for simulating the internal field [3]. The stress–strain state requires an order of magnitude fewer harmonics but that is only important than no fluid dynamics analysis is intended, which is not the case in the present work. We therefore assume that 300 harmonics are needed to simulate the diffraction pressure, and 150 to simulate the radiation pressure, both external and internal.

We also mention that the terms in the shell equations that are multiplied by k_0^2 represent the bending stiffness. As was demonstrated in [4], and further elaborated in [16], neglecting the bending stiffness does not result in significant changes of the hydrodynamic field when the shell is very thin ($h_0/r_0 \leq 0.01$). Since the objective of the present study is to see how the internal wave pattern is altered when a core is present, the second-order effects due to the bending stiffness are not particularly important. Thus, we neglect the bending stiffness and assume that the results reported here are only completely valid for shells with $h_0/r_0 \leq 0.01$. Such results would give a good qualitative idea about the interaction for thicker shells as well [4,16], although quantitative estimates of the maximum pressure could be quite a bit off.

5. Results and discussion

We consider a steel shell with $h_0/r_0 = 0.01$, $c_s = 5000$ m/s, $\rho_s = 7800$ kg/m³, and $v = 0.3$ submerged into and filled with water, $c_e = 1400$ m/s and $\rho_e = 1000$ kg/m³. We also consider a shock wave with a relatively distant source (located at the distance of five radii of the shell from the axis of the shell). The linear model used here is most suitable for modeling such an explosion [3,14] because for an explosion with a closer source the interaction starts to be dominated by nonlinear effects. The rate of the exponential decay λ and peak pressure in the front p_α are chosen to be 0.0001314 s and 250 kPa, respectively.

Four different radii of the core are considered: $a/r_0 = 0.10$, 0.25, 0.50, and 0.75. The first three are chosen to be consistent with the earlier structural analysis of [2] where they were termed small-, medium-, and large-radius cores. The last one is chosen to illustrate what happens when the core dominates the internal volume, and thus the internal fluid starts to act as a fluid layer. The main objective of this section is to see exactly how the internal pressure pattern evolves when the radius of the core increases, thus explaining why a considerable stress reduction was seen in [2] for $a/r_0 = 0.50$ but not for $a/r_0 = 0.25$ and 0.10.

It seems appropriate to use the same terminology as was introduced in [3], i.e. talk about downstream propagation (or early interaction), reflection and focusing (mid-interaction), and upstream propagation and secondary reflection and focusing (late interaction). This time, however, the reasoning for dividing the interaction in these three stages is somewhat different. Namely, the analysis of the wave pattern during the downstream propagation allows one to see how significant the influence of the core on the internal pressure wave is, thus clarifying the origins and dynamics of the high tensile stress caused by it in the tail region. Analyzing the mid-interaction will provide information about the core reflection effects, as well as the transition of the respective waves outside the shell. It will also allow one to see if the core is large enough to prevent the focusing from occurring. Finally, analyzing the late interaction allows for the understanding of the fully developed core-reflected wave pattern both inside and outside the shell.

We start with the analysis of the smallest core, $a/r_0 = 0.10$, Fig. 3, but first, for the reference purposes, include a snapshot sequence for the no-core case, Fig. 2. In the images displayed, the distribution of the grayscale was chosen individually for every snapshot in order to ensure that all the features of the hydrodynamic fields are shown in the best way possible. The pressure interval shown is displayed in the bottom left corner of every snapshot in kPa, with black corresponding to the lowest pressure and white to the highest (there are some exception to this convention in cases where a narrower pressure range ensured better visibility of certain important phenomena; in such situations, regions falling below the

lowest pressure appearing in the legend are shown in black and the ones above the highest are white). The value of the dimensionless time is shown in the bottom right corner.

The beginning of the process is identical to the no-core case, and the internal wave is not affected by the core until relatively late in the interaction, $t=0.90$. Then, the scattering of the wave by the core begins, and the classical diffraction pattern observed many times both experimentally (e.g. [19]) and numerically (e.g. [20,21]) develops. The radius of the core is small, and not all the details of the diffraction process are clearly detectable in this case; a larger core will allow for the typical diffraction features to be much better observed. Also, due to such a small radius of the core, by the time the upstream-propagating scattered wave reaches the shell surface, we effectively observe the far-field, large-time diffraction pattern (the instants of about 10 times larger than the time necessary for the wave to move over the core).

As for the influence of the core on the front of the internal wave, it is very insignificant. For all practical purposes, we can say that by the time the internal wave reaches the tail region ($t=2.00$), the disturbance due to the presence of the core
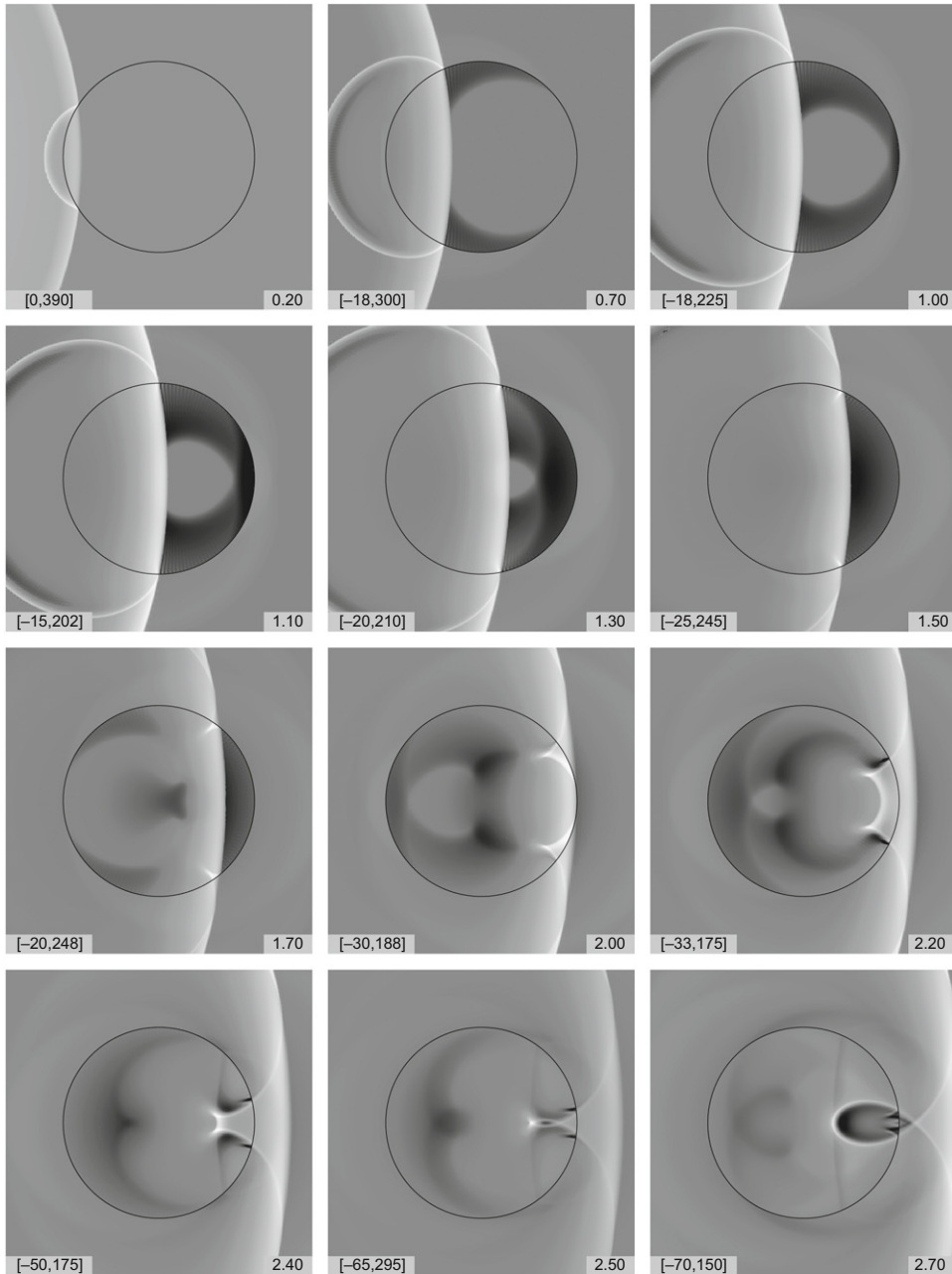
Fig. 2. Evolution of the hydrodynamic field in the absence of the core.
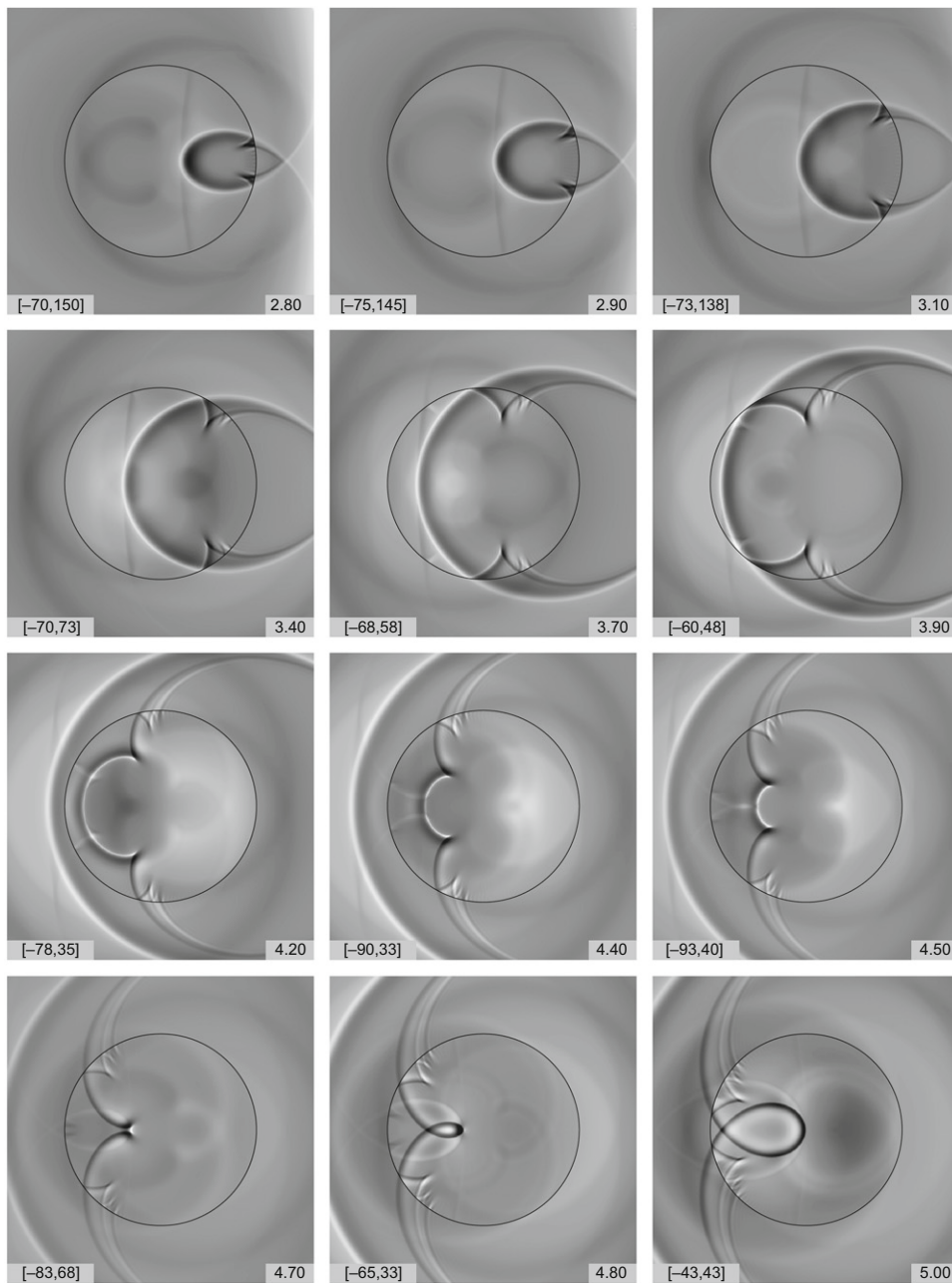
Fig. 2. (*Continued*)

is negligible. This is exactly why almost no difference in the stress–strain state was noticed between the present and no-core scenarios in [2]. Although this is an expected and rather obvious result, seeing the snapshots of the actual wave is certainly helpful.

It is worth noticing that the geometry of the scattered wavefront is nearly identical to that of the shell surface at the time of incidence ($t=1.80$). Due to this similarity, the reflected wave behaves almost like an axisymmetric wave converging in a cylindrical cavity, a phenomena that is certainly worth mentioning. Actually, the reflected wave behaves very much like a converging wave all the way up to $t=2.70$, when it is almost converged and about to focus. However, due to the presence of the core, the focusing does not take place. Instead, the wave reflects off the core once again, and starts to propagate towards the shell, snapshots for $t=2.80$ and 2.90. Since in this case there is no near-linear wavefront that was present during the initial downstream propagation of the internal pressure wave, the scattering pattern is quite different from the classical diffraction pattern, and more resembles the radiation by an empty submerged shell [14].

The diverging wave propagates towards the shell surface where it reflects at $t \approx 3.60$, and the reflected wave starts to converge again, $t = 3.70 - 4.50$. The magnitude of the respective pressure, however, is much lower than that in the primary (shell-reflected) waves, and thus the wave has little influence on the stress–strain state. Nevertheless, the near-circular and almost concentric front is still clearly detectable, and if not for the core, the wave would have converged. Instead, it reflects off the core once again at $t \approx 4.50$, and starts its passage towards the shell.

We also note that later in the interaction, all other wave-reflection phenomena inherent to the no-core scenario remain almost completely intact. Specifically, the reflection and subsequent focusing of the internal wave at $t \approx 2.50$ are not at all affected by the core because of its small radius. The same is true for the phenomena taking place later in the interaction – the upstream propagation and focusing of the shell-reflected wave is largely unaffected by the core, neither is the development of multiple regular reflection along the shell's walls. Therefore, in this case, the interaction is qualitatively very similar to the no-core scenario. On the other hand, although the core-induced waves have much lower pressure
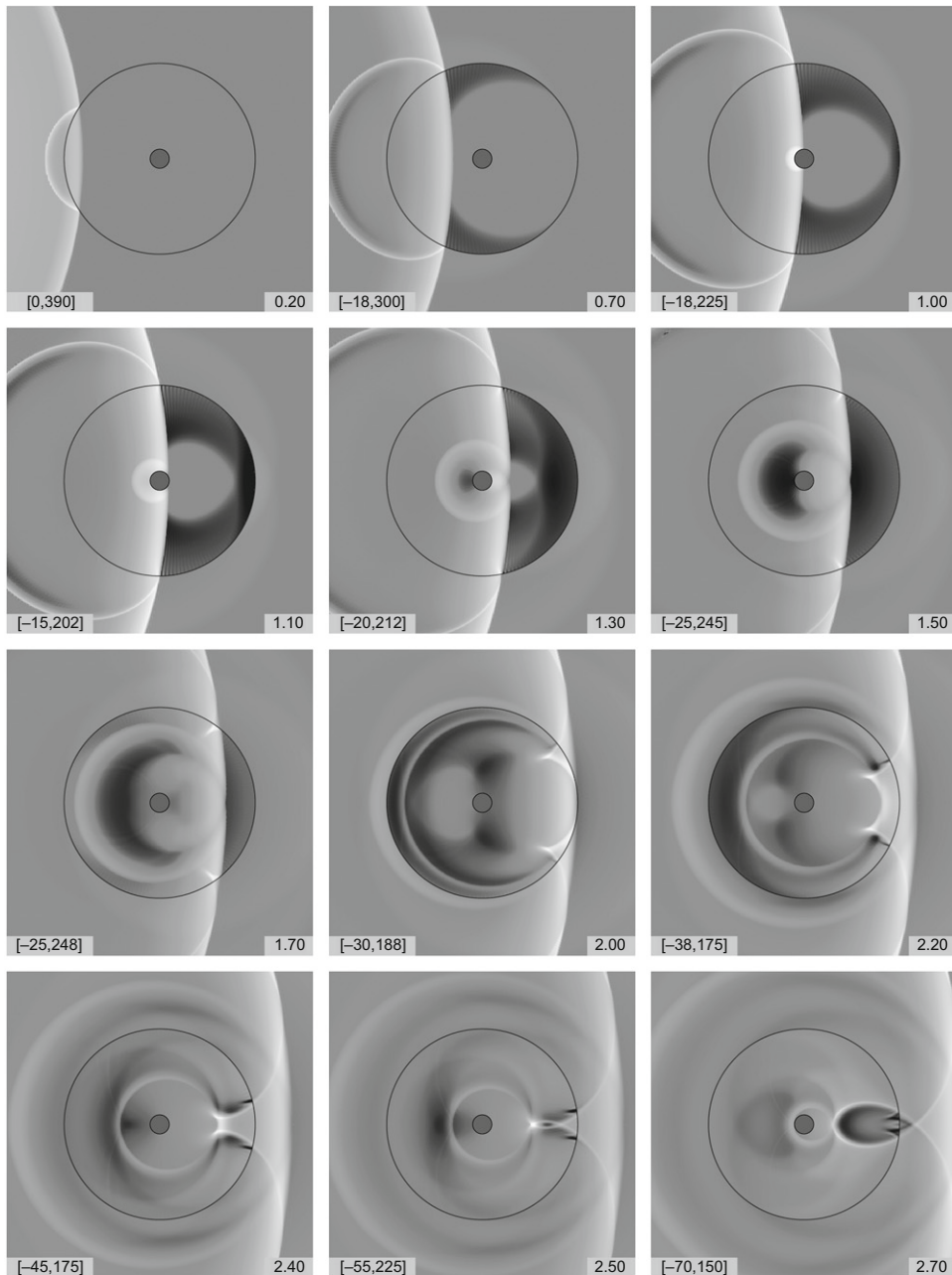
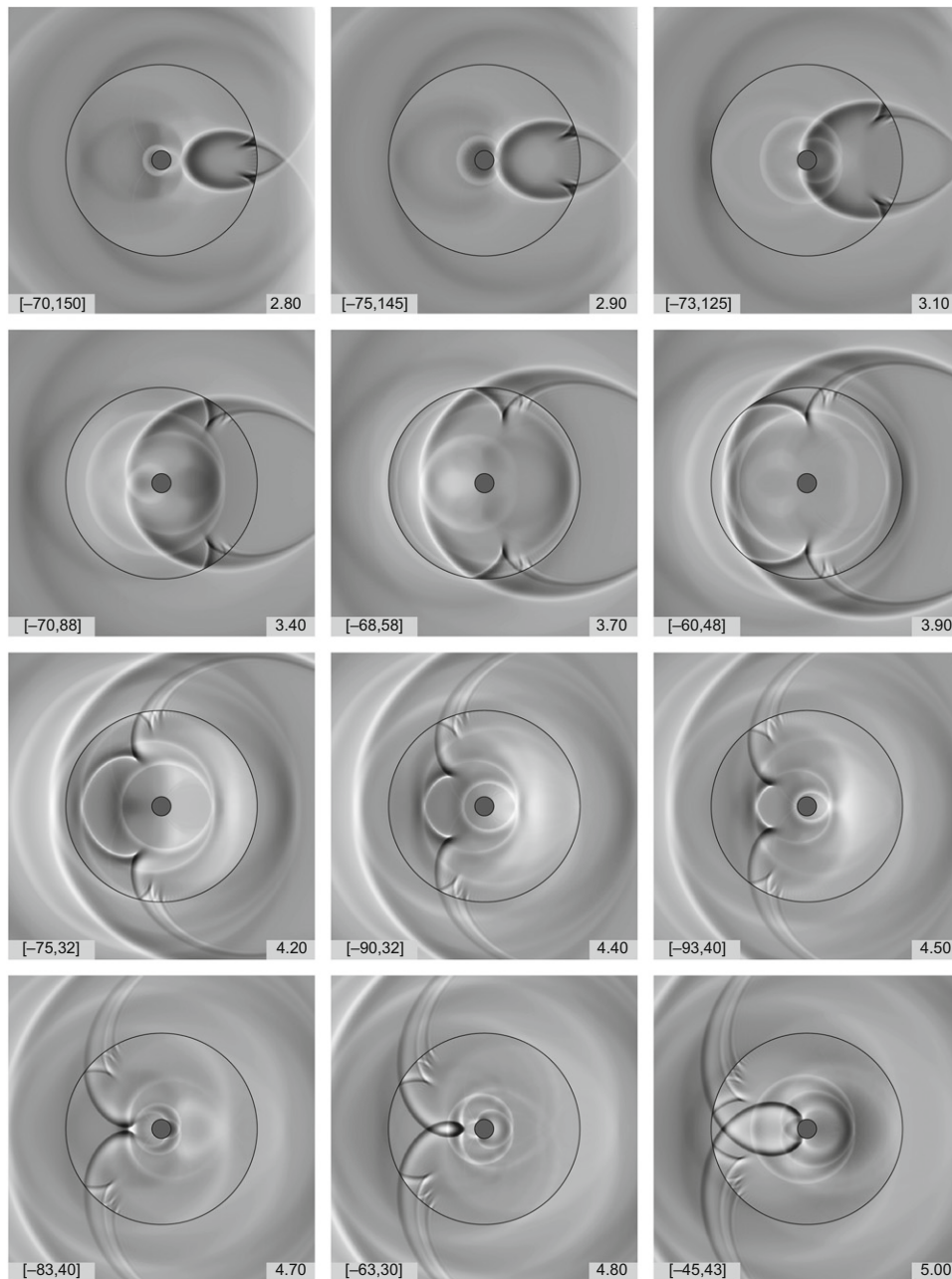**Fig. 3.** Evolution of the hydrodynamic field for $a/r_0 = 0.10$.

Fig. 3. (*Continued*)

magnitude than the 'primary' shell-reflected waves, and despite the fact that their structural effect is not significant, the internal pressure pattern is considerably more complex than in the no-core case.

The second core size we address is $a/r_0=0.25$, Fig. 4. Although the internal wave still reaches the core with a relatively large delay (at $t=0.75$), the core is large enough for the scattering pattern to show all the features of the classical diffraction in full detail. Yet, it is small enough for the diffraction field to develop sufficiently prior to the reflection off the shell surface at $t \approx 1.50$. We therefore observe in this case pressure patterns inherent to the mid-field scattering off a cylinder. At the time the scattered wave reaches the shell at $t \approx 1.50$, the pressure in it is still high enough, and the transition of the well defined, relatively high-magnitude front into the external fluid is clearly seen in the snapshots for $t=1.70$, 1.90 and 2.00.

The front of the internal shock wave is still quite close in shape to what is observed in the no-core case, thus the difference is the stress–strain state is still insignificant. It, however, does have a small irregularity of the geometry, and is also less uniform in terms of the pressure magnitude, which is why a number of secondary effects unique for this case are observed in the stress–strain state. The core still has no effect on the Mach stems and the regular reflection that starts to

develop along the walls. The shell-reflected wave starts to propagate towards the centre and exhibit a pattern similar to a converging wave, $t=2.10$. However, in this case the core is large enough to terminate the convergence a way before the focusing could begin, $t=2.40$.

The primary focusing of the internal wave still takes place as well at $t \approx 2.50$ for the core not being large enough to interfere. The secondary focusing, however, is considerably affected, $t=4.70$, with the core surface being located very close to the point where the focusing occurs in the no-core case. We can therefore conclude that as the radius of the core increases, some of the shock wave reflection and focusing phenomena inside the shell no longer take place. It does not, however, imply that the interaction becomes less complex as other wave reflection effects not seen in the no-core case become present, and more and more numerous and pronounced as the core radius increases.

We note that even the secondary core-reflected wave is still of noticeable magnitude, $t=2.90$ for example. In particular, after it reflects off the shell at $t=3.00$, it starts to converge again, $t=3.70$, but, like the primary one, its convergence is
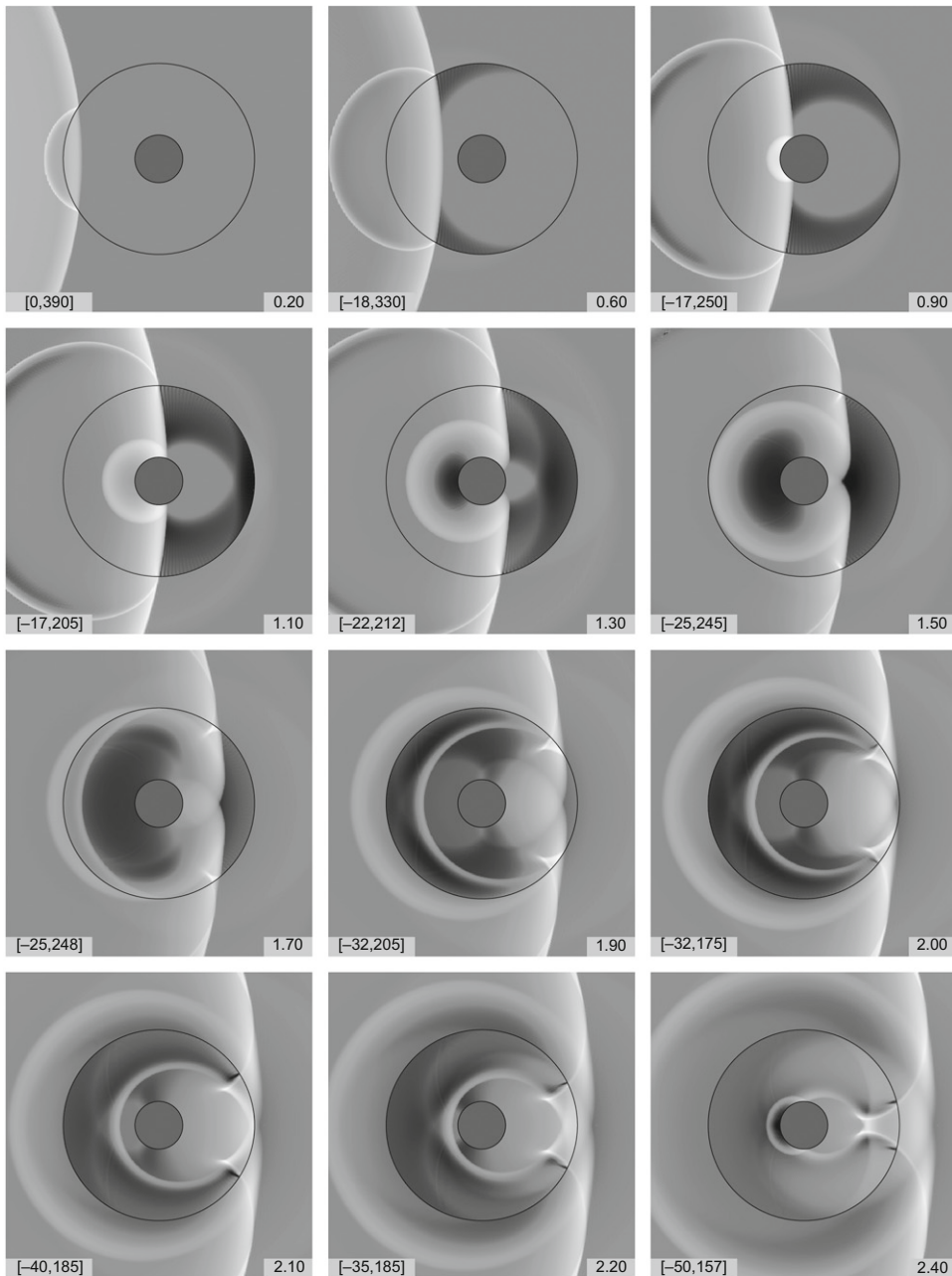

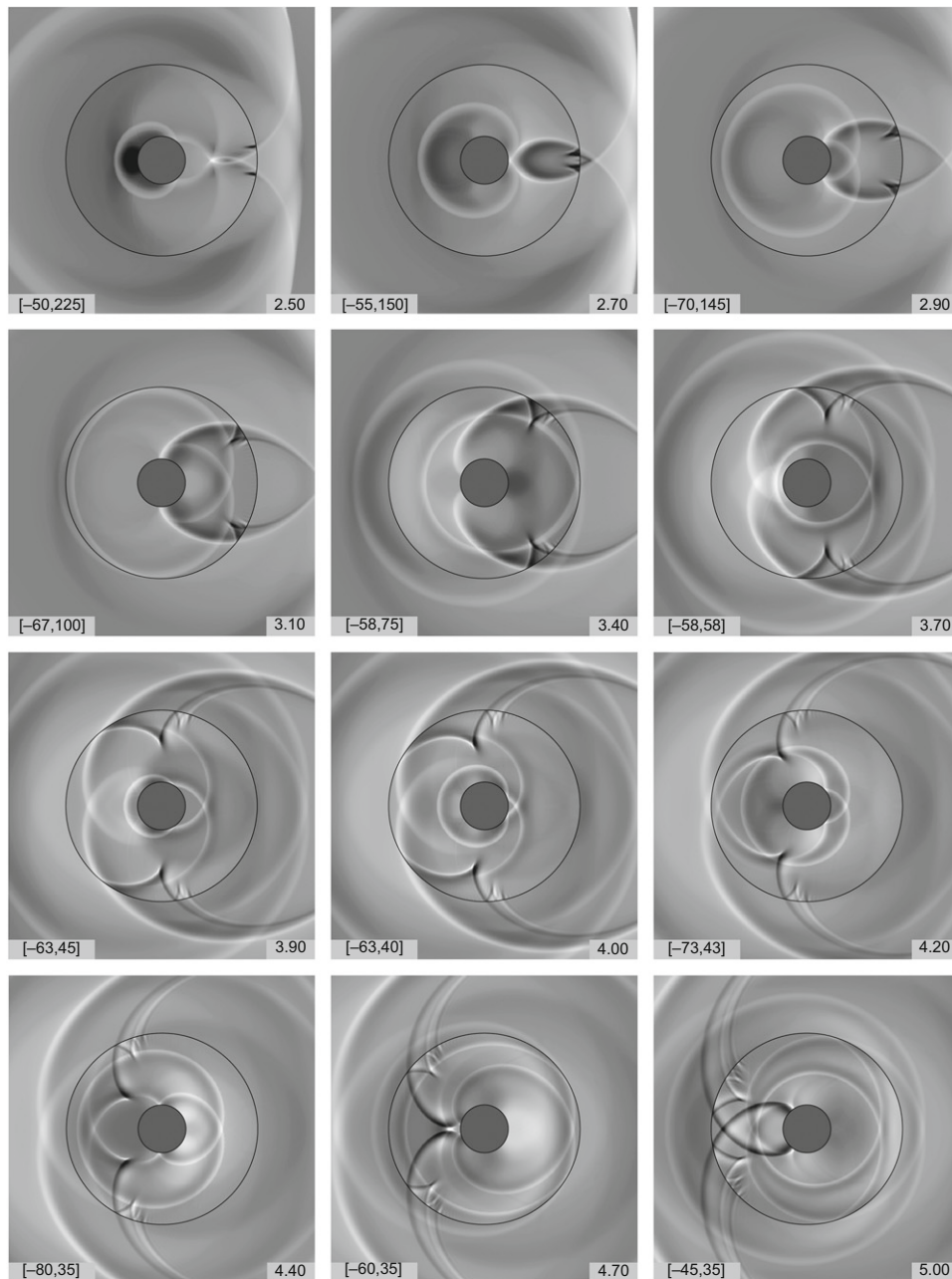**Fig. 4.** Evolution of the hydrodynamic field for $a/r_0=0.25$.

Fig. 4. (*Continued*)

terminated by the core long before the focusing could be observed. The tertiary core-reflected wave is then clearly detected to propagate towards the shell, e.g. t=4.20.

The third core size we look at is a/r_0=0.50, Fig. 5. In this case, finally, the core starts to have a significant effect on the overall internal wave pattern. The pressure in the primary core-reflected wave is significant and comparable with the pressure of the reflection of the incident wave off the shell. It impinges on the shell from at t=1.00, thus having a very pronounced influence even during the early interaction. The high-magnitude transition into the external fluid is also apparent, for example t=1.20.

Unlike for the previous two scenarios, the shell-reflected wave does no longer produce a converging pattern, but instead a concave front, t=1.20 and 1.50, that looks very much like the internal wave for the no-core scenario where the internal fluid has a lower acoustic speed than the external one [18]. Thus, the geometry of the wave propagating between the core and shell becomes qualitatively different when the core radius is large enough. The wave reflects off the core again, and

another high-magnitude wave propagates towards the shell, e.g. t=1.70. This secondary core-reflected wave clearly dominates the internal field even at t=2.00.

Since the core is now large enough to significantly alter the shape of the front of the internal wave, the impact of the latter on the tail region is dramatically reduced. Namely, what used to be a very uniform high-magnitude front that impinged on the shell at $t \approx 2.00$, now has a non-uniform structure represented by two individual, rather high-curvature branches, complemented by two high-pressure regions adjacent to the walls and associated with the Mach stems. There is no longer a precise 'impact instant', but more like an 'impact interval' when the transition of the non-uniform internal front into the external fluid occurs, $t \approx 2.00-2.20$. Thus, there is no direct 'hit' by the internal wave, and this is exactly why the tensile stress at the tail point is so much lower in this case. Thus, we can state that we have finally clarified why a dramatic reduction of the tensile stress was seen for a/r_0=0.50 in the 3D study of the stress–strain state dynamics of the system [2].
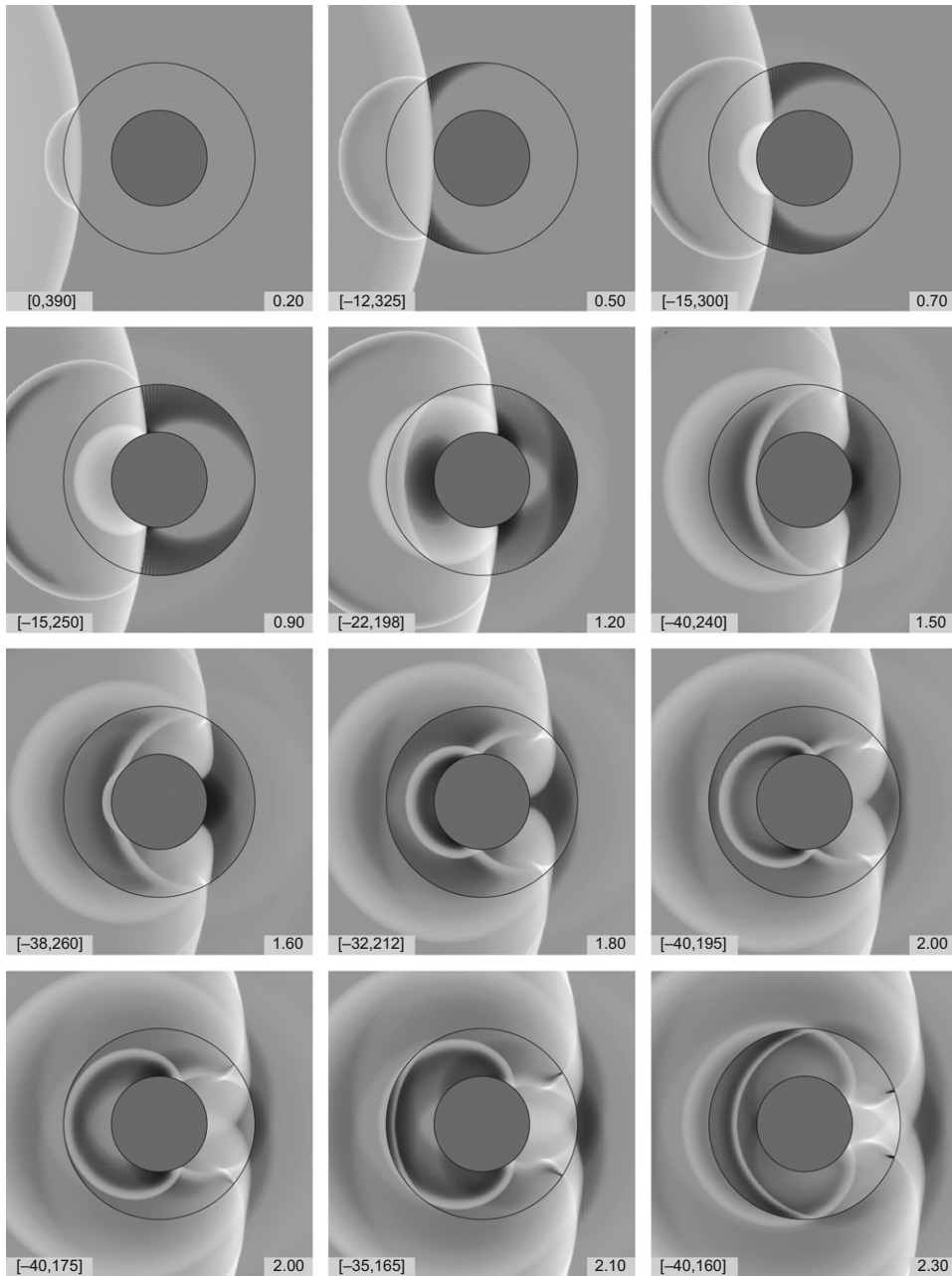

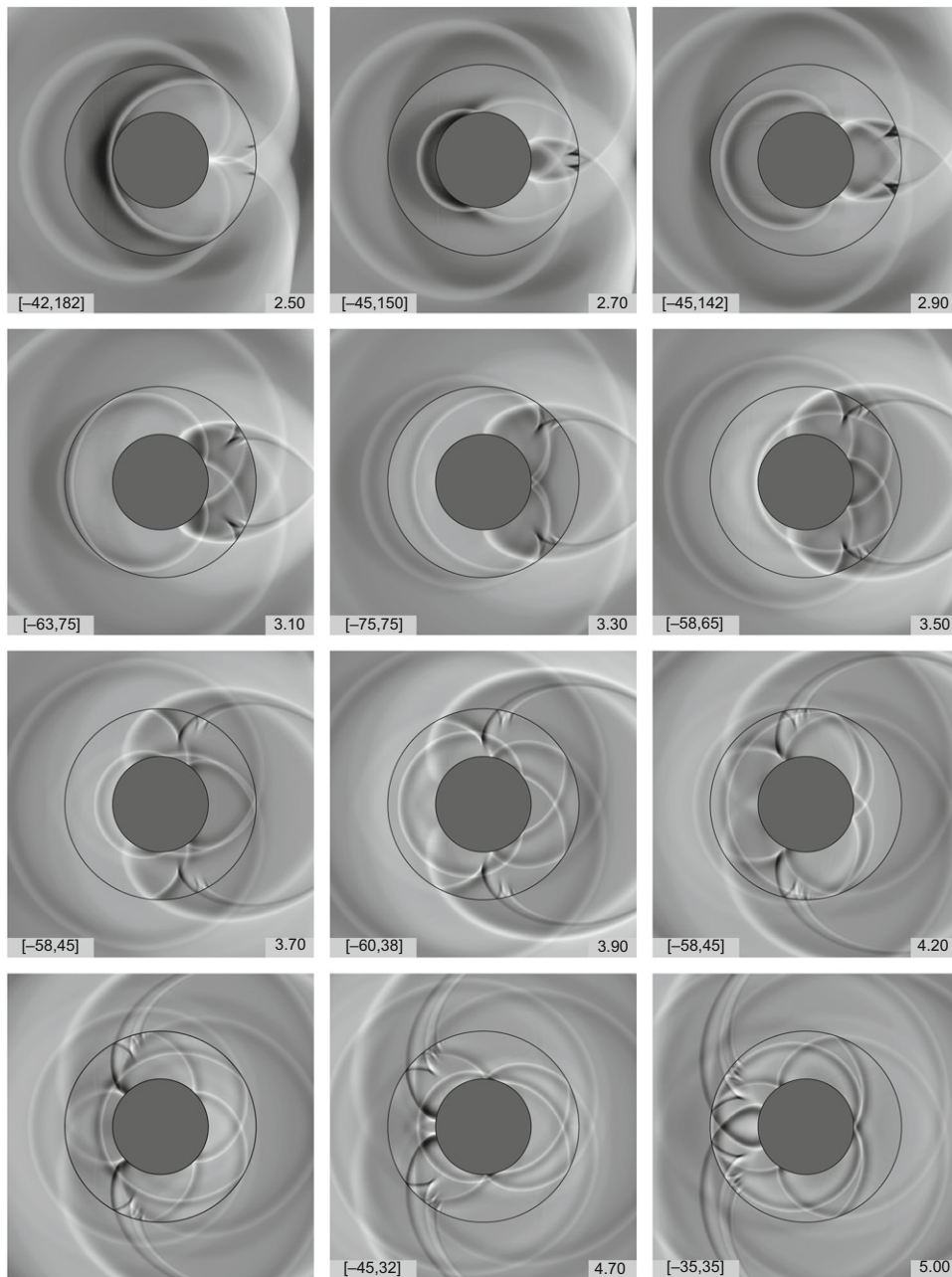**Fig. 5.** Evolution of the hydrodynamic field for a/r_0=0.50.

Fig. 5. (*Continued*)

It is not only the internal wave that is dramatically affected by the core: nearly every other shock wave propagation and reflection phenomenon is affected as well. Most noticeably, the primary focusing of the internal wave occurs right on the surface of the core, $t \approx 2.50$, and if the core were just a bit larger, the focusing would not take place at all. This, by the way, also indicates that when the core radius is close to 0.50, it experiences very high pressure (exceeding the incident pressure on the shell surface [3]) quite late in the interaction, a point that can be of interest for certain systems. The post-focusing pattern is, expectedly, very different from the no-core case.

The mid-interaction is dominated by two groups of phenomena – the effects associated with the post-focusing upstream propagation of the internal wave (similar to the no-core case), and the multiple reflections of the wave between the core and shell (unique to the scenario with a core). The interplay between the two induces a multitude of lower-order interactions, and results in a complex and very interesting-looking pressure patterns, e.g. $t = 3.50$ and 3.90. It is interesting to point out that although most of the internal pressure pattern is completely different from the no-core case, the pressure

in the near-wall regions still exhibits all the main features seen when no core is present, for example the multiple regular reflection clearly seen at t=4.00.

The late interaction is even more complex and diverse in terms of the variety of phenomena observed than the mid-interaction, e.g. t=4.40 and 4.90. No secondary focusing is observed, but most of the features of the multiple regular reflection pattern are still present. As was the case with the no-core system, the transition of the multiple Mach stems into the external fluid is observed here as well. However, the corresponding external field is now complemented by many other waves of different magnitude and geometry, thus making a shell with a larger core an extremely interesting acoustical source.

We finally consider the scenario of a/r_0=0.75, Fig. 6. In this case, the core dominates the external volume, and its presence determines nearly every aspect of the interaction. In fact, for such a large core it may even be more appropriate to refer to the internal fluid volume as a 'fluid layer'. Even the early interaction is significantly affected, with the primary core-reflected wave arriving at the shell as early as t=0.50.
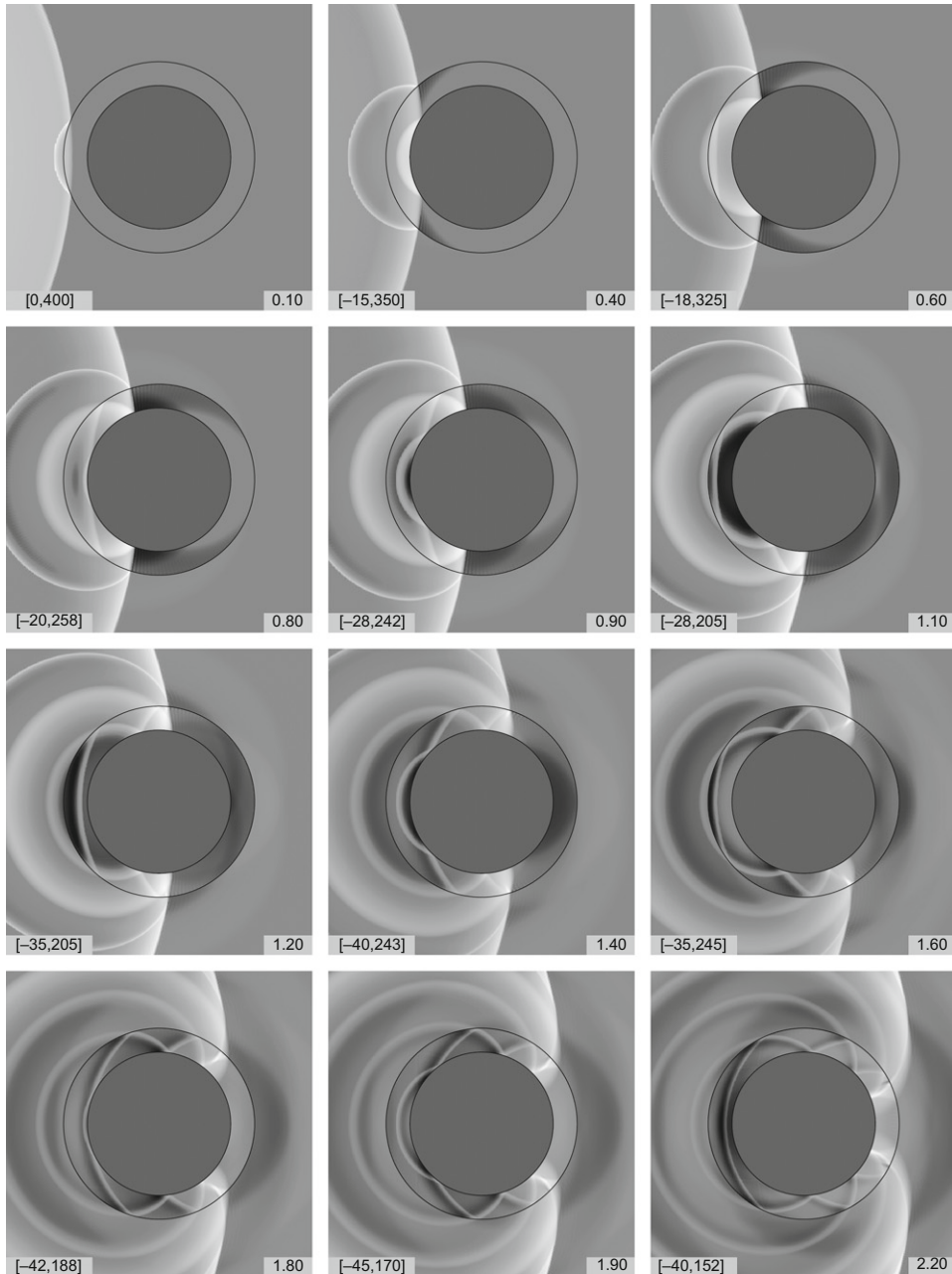

Fig. 6. Evolution of the hydrodynamic field for a/r_0=0.75.
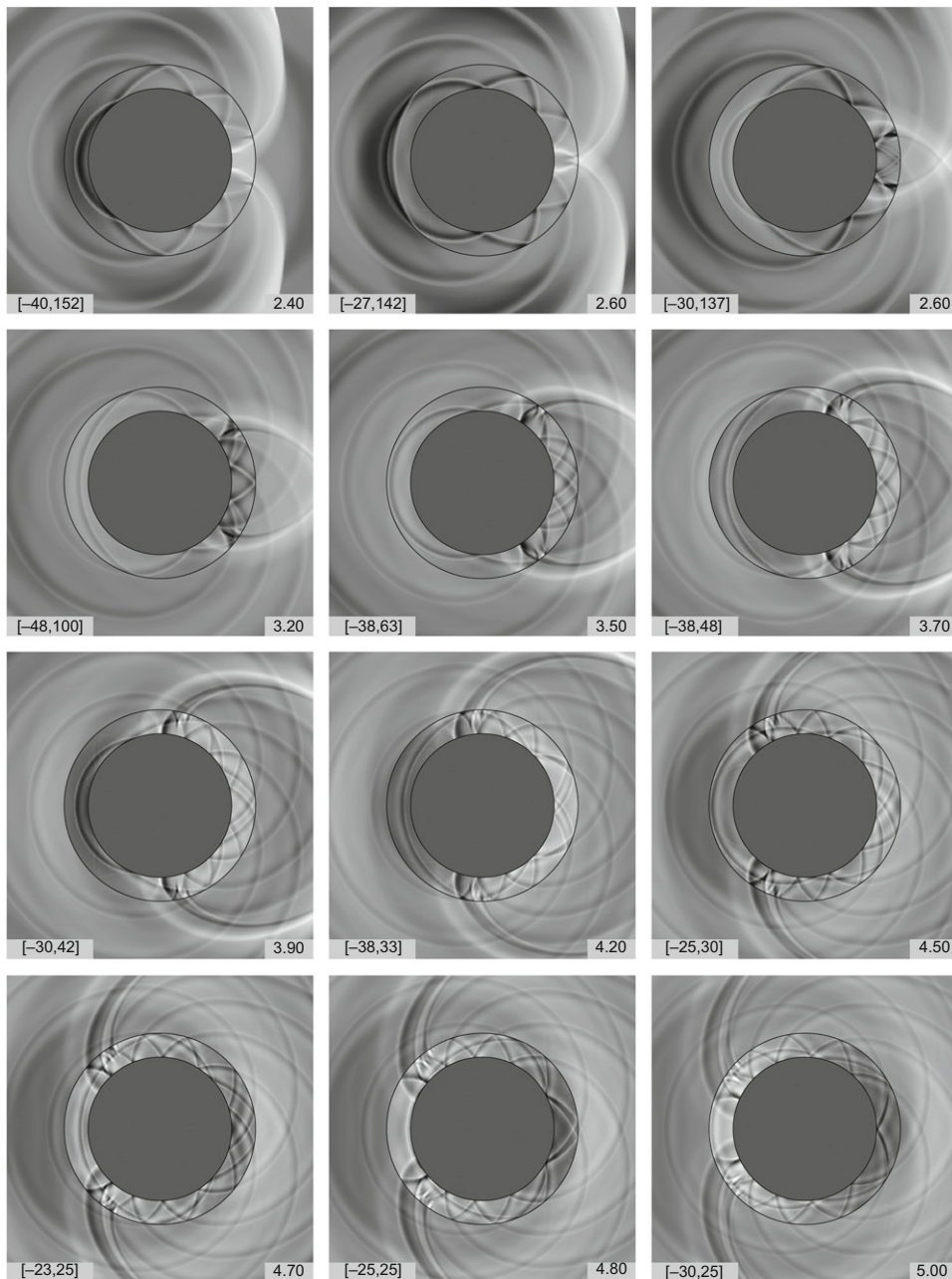
Fig. 6. (*Continued*)

The interaction is dominated by the constant reflection of the internal wave from the core and the shell, with the transition of the respective waves into the external fluid (because the clearance between the core and the shell is so small, every reflection off the shell surface induces a high-magnitude wave in the external fluid, e.g. t=0.50, 1.00, 1.50, and 2.00). As a result, there is a system of waves of very similar geometry propagation in the external fluid, all of them uniformly spaced with the dimensionless distance between the fronts of 0.50. It is interesting to point out that, at the same time, the geometry of the wave that 'bounces' between the core and shell surface changes as the interaction progresses, compare the snapshots for t=0.90 and 1.90.

Although there still exists the portion of the internal wave that nominally corresponds to the front of the internal wave in the no-core case, it is not extensive, and does not play any particularly significant role in the overall wave pattern. It does lead to the Mach stems developing near the shell surface, but they are considerably less pronounced than before, and are very significantly affected by other waves (compare, for example, the snapshot for t=1.90 in the present case to that for

a/r_0=0.25). As a result, there is no 'hit' at the tail point associated with the internal wave at all, only a smooth transition of different segments of it into the external fluid at t=2.10−2.60. This is, of course, clearly reflected in the dynamics of the stress–strain state which is dominated by the multiple reflections of the internal wave, as opposed to a few singular effects of the no-core scenario.

Both primary and secondary focusings no longer exist, and the only feature of the classical internal reflection that is still present is the multiple regular reflection observed during the late interaction. As long as the respective Mach stems are compact enough not to interfere with the core, they continue to exist in the near-wall region.

Another result of the multiple reflections off the core and the shell is that it looks as though the front of the internal wave seen in the no- or small-core cases is now broken into many pieces and 'wrapped' around the core, e.g. snapshot for t=1.90. This prompts an analogy with a waveguide, in a sense that the internal fluid layer can very well be referred to as a 'waveguide' that carries the energy of the initial impact towards the tail region, and that also conveys upstream the wave system formed when the downstream-propagating waves superposed at the tail point.

This waveguide analogy allows us to go one step further and say that there now are similarities between the reaction of the shell to the initial impact of the incident wave, and the response of the internal fluid. Namely, the shell, as an elastic medium, conducts a variety of elastic waves that circumferentially propagate around the shell and radiate into surrounding fluid(s) [3,4,13,17]. Now, in a similar manner, the fluid layer conducts circumferential waves that, although transmitting into the external fluid, are mostly confined inside the layer itself. Strictly speaking, we would need to look at a fluid layer confined between two elastic media to be able to say that we observed the exact opposed of a submerged fluid-filled shell, the analogy noticed still appears to be of interest.

When the waves superpose at the tail point at $t \approx 2.60$ and start to propagate upstream, the wave pattern becomes even more complex than during the downstream propagation, e.g. t=3.50, 3.70 and 4.20. The reflection of the multitude of the internal waves is accompanied by their constant radiation in the external fluid, and the result is a complex, although quite uniform and relatively easily interpretable, external wave pattern. It is also quite beautiful, at least in the authors' opinion, and resembles images that are often referenced in talks and papers reflecting on the connection between mathematics and art, in particular the snapshots for t=4.50 and 4.70. The existence of a pattern like that is also a clear illustration of just how complex a source a shell with a large core is from the acoustical point of view.

Now, having addressed in some detail the hydrodynamic fields of the interaction, we would like to make some remarks on the respective stress–strain states. More specifically, we would like to further discuss the reduction of the peak tensile stress observed when a core is present, the phenomenon that, as we highlighted earlier, was one of the primary motivations for this study. Fig. 7 shows the transverse stress at the tail point $\theta = \pi$ for the four considered cores in the present 2D case. A dramatic reduction of both tensile stress peaks is obvious for the largest core, a/r_0=0.75. Also, as
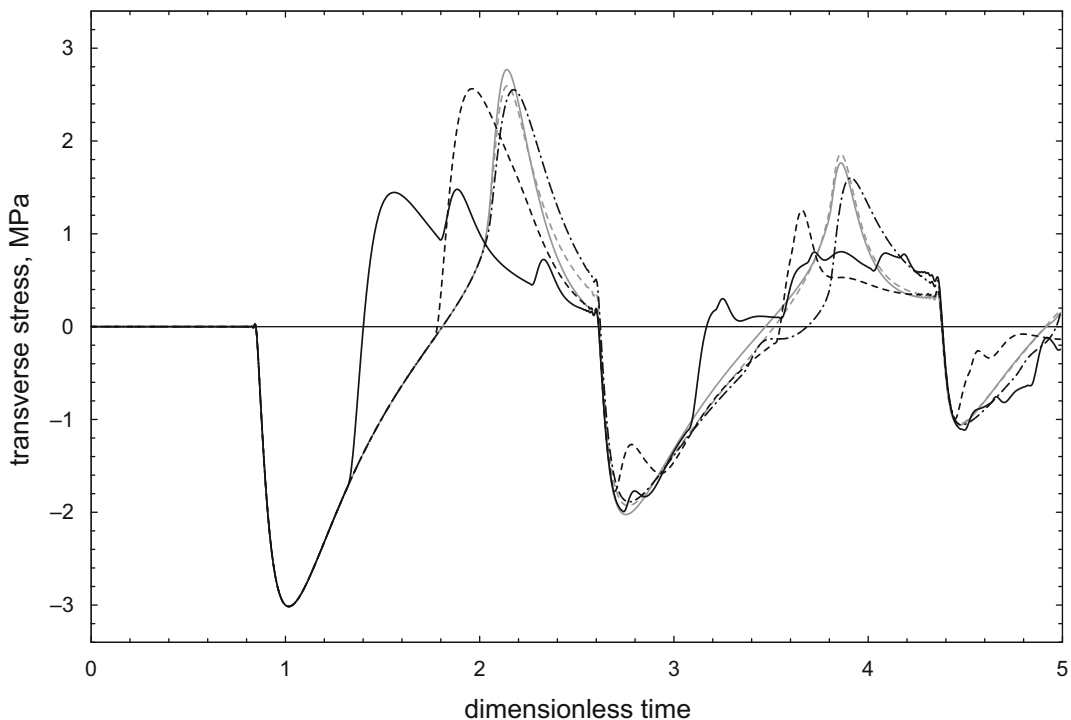
Fig. 7. Transverse stress at the tail point $\theta = \pi$ in the 2D case in the absence of the core, solid gray line, and for the four cores of different radii: a/r_0=0.10, dashed gray line; a/r_0=0.25, dashed-dotted line; a/r_0=0.50, dashed black line; and a/r_0=0.75, solid black line.
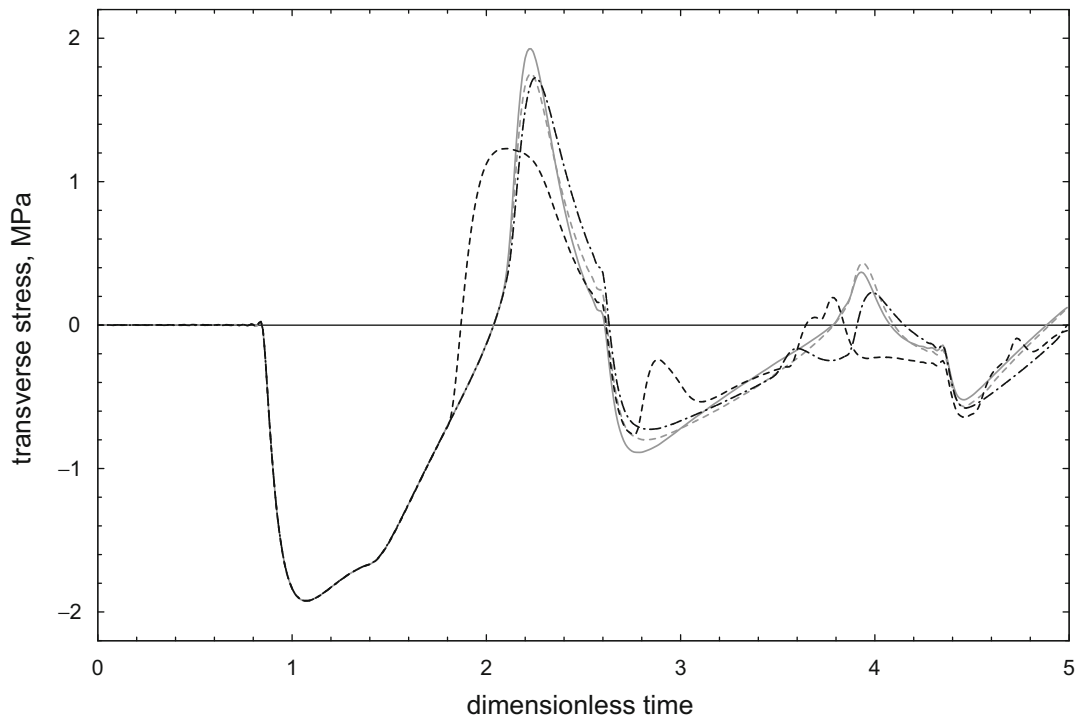
Fig. 8. Transverse stress at the tail point $\theta = \pi$ of the middle cross-section in the 3D case in the absence of the core, solid gray line, and for the three cores of different radii: a/r_0=0.10, dashed gray line; a/r_0=0.25, dashed-dotted line; and a/r_0=0.50, dashed black line.

expected, the smallest core, a/r_0=0.10, has little effect on the peak tensile stress, as does the core next in size, a/r_0=0.25. These observations are consistent with what was seen in the 3D case in [2]. However, the situation for the case of a/r_0=0.50 is different: a significant stress reduction seen in the 3D case, Fig. 8, is not observed at all, instead, a peak stress that is slightly higher than that for the case of a/r_0=0.25 is detected (note that the core with a/r_0=0.75 is not shown in the 3D case).

In order to understand the reasons for such a discrepancy, we need to recall the rather essential difference in the incident loads in the 2D and 3D models used. Namely, in the 2D case we study the effect of a wave that has no longitudinal variation associated with it, thus no longitudinal dissipation occurs at any time. In the 3D case, however, the incident wave is spherical, and as a result of that, the longitudinal dissipation occurs at all times. We believe that it is this difference that is responsible for the discrepancy seen in the peak stress reduction. The apparent difference in the magnitude of the peak stresses observed in the 2D and 3D cases further supports this explanation, and particularly so the difference in the magnitude of the secondary peaks. We note that although the 2D case exhibits a less dramatic reduction of the peak stress than its 3D (and, thus, more realistic) counterpart, the present analysis of the hydrodynamic fields is still valuable since it is expected that, as was discussed earlier, the most important features of the process are similar in the 2D and 3D cases.

Finally, it seems appropriate to comment on the computational efficiency of the methodology developed. We chose an approach where the computational procedure was divided into a number of steps, each focusing on a specific task and using a specifically developed code module. Such an approach allowed for a more efficient code development, and it also allowed for more flexibility and functionality with the data manipulating and storing. All computations were performed on an AMD Athlon 2.41 GHz dual core processor, and none of the algorithms were parallelized.

The least expensive is the computation of the displacement harmonics — it takes around 140 s to compute 150 harmonics with the time step of 0.001 (150 harmonics are assumed to be the case for all other cost estimates given below). The computation of the hydrodynamic fields is far more expensive. Namely, the computation of the internal field when no core is present costs 125 s per radial layer, or about 3.5 h per 100 layers used to create the images shown in this paper (the pre- post-processing output was done with the 0.0025 time step). These relatively high costs are due to the fact that when the core is absent, the response functions have singularities which need to be treated in a very particular way [22] to ensure an acceptable accuracy of the results. When the core is present, the response functions do not have singularities (see Appendix) and thus the computational costs are much lower, about 16 s per radial layer, or around 13 min for the entire field for a=0.50 with the step of 0.01 r-wise (the output time step of 0.001). It is assumed that the response functions have been pre-computed since they only need to be computed once for any given geometry.

The costs of the computation of the external field do not depend on the presence of the core and are always quite high. It takes 5.5 and 4.85 h to compute the external diffracted and radiated fields, respectively, for 200 radial layers spaced by

0.01, which is slightly more than is necessary to display the field in a square 4 by 4 radial units window centered at the axis of the shell, and quite a bit more than was necessary to produce the images shown here (for both fields, the output time step was 0.001). The post-processing (converting the modal form into a data file that can be read directly by a field-visualization code developed in the package Mathematica) is far less expensive, around 6.5 and 26 min for the internal (no-core) and external fields, respectively, assuming the parameters given above.

6. Conclusions

We have considered the response of a submerged fluid-filled cylindrical shell with a core to a shock wave, and simulated the respective hydrodynamic fields using the semi-analytical solution developed. Both the evolution of the pressure pattern in the fluids and the influence of the core on the stress–strain state of the shell were analyzed. Four cores were considered, a/r_0=0.10, 0.25, 0.50, and 0.75.

It was demonstrated that when the radius of the core is small (a/r_0=0.10 was considered as a representative case), it has very little influence on the shape of the front of the pressure wave in the internal fluid. As a result, the stress–strain state of the shell is very similar to what was observed for a no-core scenario. The reflection of the internal wave off the core exhibits all the features of classical shock wave diffraction, and by the time it reaches the shell, it has enough time to develop sufficiently for one to observe the far-field diffraction pattern. None of the other shock wave reflection and focusing phenomena observed in the internal fluid in the no-core case are affected either.

For a larger core, a/r_0=0.25, its influence on the internal wavefront is more pronounced, although it is still not large enough to cause significant changes to the stress–strain state. The primary focusing of the internal wave is not affected, but the secondary one occurs very close to the surface of the core. Most of the other features of the internal wave propagation and reflection remain unaffected. The distance between the core and the shell is still large enough for the scattered pattern to develop sufficiently, and one observes the mid-field diffraction when the core-scattered wave falls on the shell.

When the radius of the core is further increased, a/r_0=0.50, its effect on the internal pressure pattern finally becomes very significant. The front of the internal wave no longer has a uniform shape, and there is no exact 'impact instant' corresponding to the internal wave falling on the shell. This explains the dramatic reduction of the tensile stress seen for a larger core in the earlier studies. The primary focusing occurs very close to the surface of the core, and the secondary focusing is not observed at all.

Finally, when the core starts to dominate the internal volume, a/r_0=0.75, nearly every aspect of the interaction is different from the no-core case. The fluid volume between the core and the shell starts to behave like a fluid 'layer', and the process is dominated by the multiple reflection of the internal wave from the inner shell surface and the core. The reflection is accompanied by the constant radiation of waves in the external fluid, and a shock-responding shell with a large core is therefore shown to be a particularly interesting acoustic source. Along with their theoretical value, the images of the late interaction for the case of a large core appear to possess certain aesthetical appeal as well.

Acknowledgements

Appendix A. Response functions

Here, an analytical approach to the inversion of the transforms

$$\Xi_n^c(s) = \frac{I_n'(as)\,K_n(rs) - K_n'(as)\,I_n(rs)}{s(K_n'(s)\,I_n'(as) - I_n'(s)\,K_n'(as))},$$

(34)

is developed, and the originals ξ_n^c are obtained in the form of an infinite series.

The main idea is the same as in the no-core case [22]. That is, we determine the zeros of the denominator of (34), and then apply Cauchy's residue theorem to obtain the series expressions for the ξ_n^c. We first rewrite (34) for the argument is [23],

$$\Xi_n^c(\mathrm{is}) = \frac{J_n'(as)\,Y_n(rs) - Y_n'(as)\,J_n(rs)}{s(Y_n'(s)\,J_n'(as) - J_n'(s)\,Y_n'(as))},$$

(35)

where J_n and Y_n are the Bessel functions of the first and second kind of order n, respectively. The denominator of (35) only has real simple zeros ω_k^n [23], and thus all the zeros of $\varXi_n^c$ are simple and pure imaginary, $i\omega_k^n$. Thus, the situation here is very similar to that in the no-core case where all the zeros were pure imaginary as well. Using Mellin's integral and applying Cauchy's residue theorem to the integration contour consisting of a segment of a straight vertical line and an arc of a circle of the respective radius [22, Fig. 1] the inverse transforms can be obtained as

$$\xi_n^c(r,t) = \sum_{k=\pm 1, \pm 2, \dots} R_{s_k^n}^n, \tag{36}$$

where $R_{s_k^n}^n$ is the residue of $\varXi_n^c(r,s)\,e^{st}$ at the point $s_k^n = i\omega_k^n$, as well as at $s=0$ for $n=0$.

It is easy to show that each pair of residues $R_{i\omega_k^n}^n$ and $R_{-i\omega_k^n}^n$ produces a real number,

$$R_{i\omega_k^n}^n + R_{-i\omega_k^n}^n = -\frac{2\Delta_k^r \Delta_k}{\omega_k^n(\alpha_k^n \Delta_k^2 - \beta_k^n)}\,\sin\omega_k^n t, \tag{37}$$

where

$$\Delta_k^r = J_n^{'}(a\omega_k^n)\,Y_n(r\omega_k^n) - Y_n^{'}(a\omega_k^n)\,J_n(r\omega_k^n), \tag{38}$$

$$\Delta_k = J_n^{'}(a\omega_k^n)\,Y_n(\omega_k^n) - Y_n^{'}(a\omega_k^n)\,J_n(\omega_k^n) \tag{39}$$

and

$$\alpha_k^n = \frac{n^2}{(\omega_k^n)^2} - 1, \quad \beta_k^n = \frac{4}{\pi^2(\omega_k^n)^2}\left(\frac{n^2}{a^2\omega_k^n} - 1\right). \tag{40}$$

It is also easy to see that at $s=0$, the residue of ξ_0^c is

$$R_0^0 = \frac{2t}{1-a^2}. \tag{41}$$

Then, we can easily write down the final expressions for the response functions,

$$\xi_n^c(r,t) = -2\sum_{k=1}^\infty \frac{\Delta_k^r \Delta_k}{\omega_k^n(\alpha_k^n \Delta_k^2 - \beta_k^n)}\,\sin\omega_k^n t, \quad n\geq 1, \tag{42}$$

$$\xi_0^c(r,t) = \frac{2t}{1-a^2} - 2\sum_{k=1}^\infty \frac{\Delta_k^r \Delta_k}{\omega_k^0(\alpha_k^0 \Delta_k^2 - \beta_k^0)}\,\sin\omega_k^0 t. \tag{43}$$

We note that using the asymptotic expressions for the Bessel functions [23], it is not difficult to demonstrate that as $a\to 0$, the series expressions (42) and (43) become the respective expressions for the response function ξ_n^i that appear when no core is present ($a=0$, [22]).

The behavior of the functions ξ_n^c is of particular interest since it has been demonstrated [2,3,16] that the response functions capture the most essential features of the behavior of a shell-fluid(s) system interacting with a non-stationary loading. A discussion of the 'surface' counterparts of ξ_n^c can be found in [2], and here we address the general case of $a \leq r \leq 1$ (i.e., the response everywhere inside the fluid layer between the core and the shell).

The first and most distinct difference between the present and no-core [3] cases is that the functions ξ_n^c do not have any singularities, Figs. 9 and 10, whereas the functions ξ_n^i have infinitely many of them. This is due to the fact that the presence of the singularities of the response functions in the no-core case was determined by the multiple focusing of a converging axisymmetric pulse at the center $r=0$. Now that the core isolates the center, the pulse no longer focuses there but merely reflects off the core at $r=a$.

As was the case for the ξ_n^i, surface reflections correspond to finite discontinuities of ξ_n^c. However, since there now are two reflective surfaces (the shell and the core), the frequency of the occurrence of the surface reflections is twice as high anywhere inside the fluid — any point inside the fluid domain 'feels' the pulse twice on its way to and from the core, Fig. 9, $r=0.7$ and 0.8. At the shell and core surfaces, the functions only have one discontinuity for each passage of the pulse between the shell and core, Fig. 9, $r=0.5$ and 1.0. Note that at $r=a$ (i.e., at the core) the function is equal to unity, whereas at $r=1.0$ (at the shell surface) it is zero, and becomes non-zero for the first time only at $t=a$. This is due to the fact that the pulse originates at the shell surface at $t=0$, then travels towards the core and arrives at its surface at $t=a$.

As n increases, the behavior of the response functions becomes more irregular, Fig. 10. In particular, the frequency of oscillations between the points of discontinuity increases, while the locations of the points themselves do not change. Also, as a increases, the number of points of discontinuity in the time interval of interest increases as well, Fig. 11. This is expected, of course, because the time needed for the wave to travel from the shell to the core and back gets smaller and smaller as a increases.
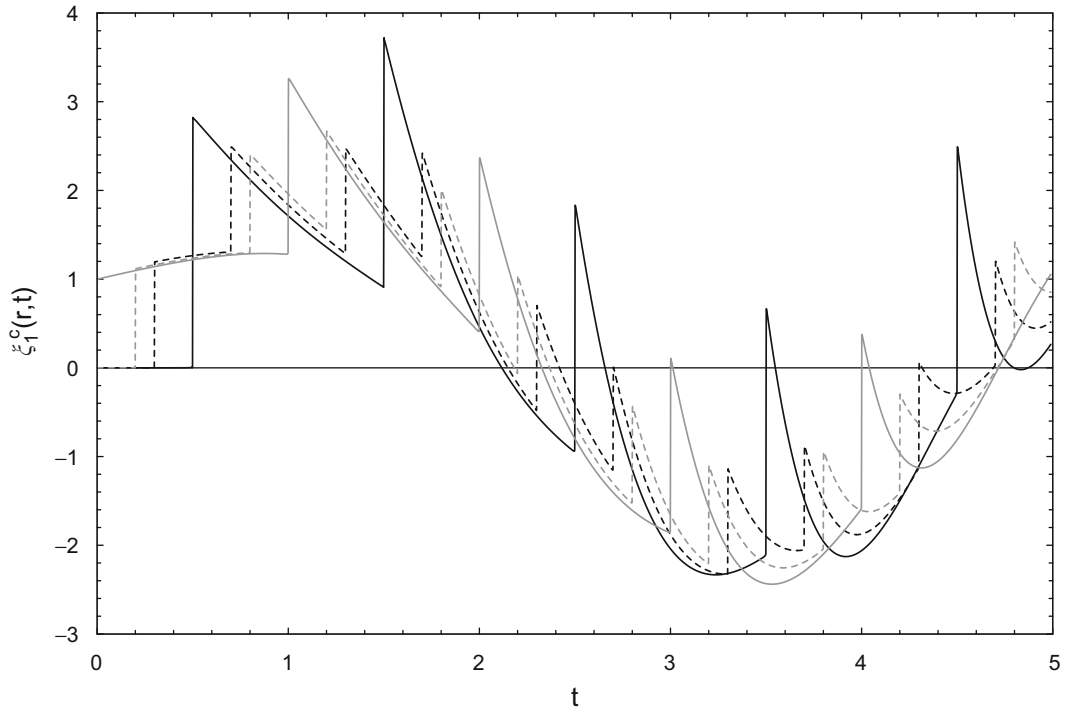
Fig. 9. Internal response function $\xi_1^c(r,t)$ for $a=0.50$ and various r: $r=0.50$, solid black line; $r=0.70$, dashed black line; $r=0.80$, dashed gray line; and $r=1.00$, solid gray line.
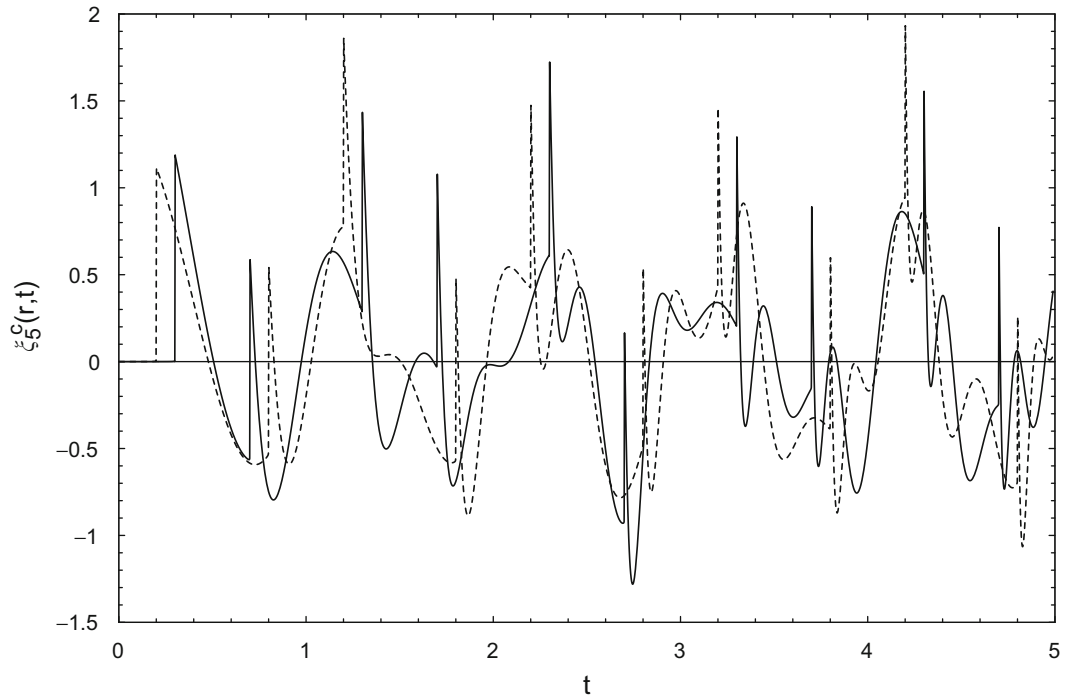
Fig. 10. Internal response function $\xi_5^c(r,t)$ for $a=0.50$ and two different values of r, $r=0.70$, solid line, and $r=0.80$, dashed line.
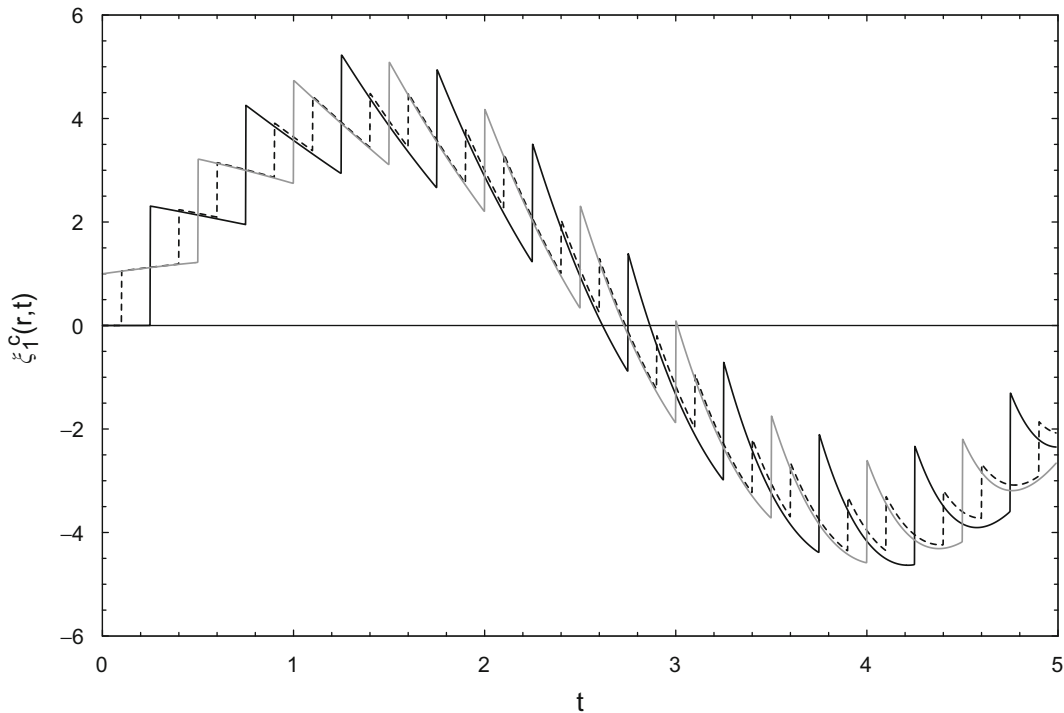
Fig. 11. Internal response function $\xi_1^c(r,t)$ for $a=0.75$ and various r: $r=0.75$, solid black line; $r=0.90$, dashed line; $r=1.00$, solid gray line.

References

[1] C. Leblond, J.F. Sigrist, B. Auvity, H. Peerhossaini, A semi-analytical approach to the study of an elastic circular cylinder confined in a cylindrical fluid domain subjected to small-amplitude transient motions, *Journal of Fluids and Structures* 25 (2009) 134–154.

[2] S. Iakovlev, Influence of a rigid co-axial core on the stress–strain state of a submerged fluid-filled circular cylindrical shell subjected to a shock wave, *Journal of Fluids and Structures* 19 (2004) 957–984.

[3] S. Iakovlev, External shock loading on a submerged fluid-filled cylindrical shell, *Journal of Fluids and Structures* 22 (2006) 997–1028.

[4] S. Iakovlev, Submerged fluid-filled cylindrical shell subjected to a shock wave: fluid–structure interaction effects, *Journal of Fluids and Structures* 23 (2007) 117–142.

[5] H. Huang, Transient response of two fluid-coupled cylindrical elastic shells to an incident pressure pulse, *Journal of Applied Mechanics* 46 (1979) 513–518.

[6] A.B. Wardlaw, J.A. Luton Jr., Fluid-structure interaction mechanisms for close-in explosions, *Shock and Vibration* 7 (2000) 265–275.

[7] L. Jialing, N. Hongli, Study on propagation of blast wave over cylinder in a channel bend, *Proceedings of the 21st International Symposium on Shock Waves*, Great Keppel Island, Australia, July 1997, pp. 103–107.

[8] V.D. Kubenko, V.V. Dzyuba, Resonance phenomena in cylindrical shell with a spherical inclusion in the presence of an internal compressible liquid and an external elastic medium, *Journal of Fluids and Structures* 22 (2006) 577–594.

[9] S. Olsson, Scattering of acoustic waves by a sphere outside an infinite circular cylinder, *Journal of Acoustical Society of America* 88 (1990) 515–524.

[10] J.G. Oakley, M.H. Anderson, S. Wang, R. Bonazza, Shock loading of a cylinder bank with imaging and pressure measurements, *Proceedings of the 23nd International Symposium on Shock Waves*, Fort Worth, Texas, USA, July 2001, pp. 589–595.

[11] J.F. Sigrist, D. Broc, C. Laine, Fluid-structure interaction effects modeling for the modal analysis of a nuclear pressure vessel, *Journal of Pressure Vessel Technology* 129 (2007) 1–6.

[12] Y. Lu, R.J. Rogers, Instantaneous squeeze-film force between a heat exchanger tube and a support plate for arbitrary tube motion, *Journal of Fluids and Structures* 9 (1997) 835–860.

[13] C. Leblond, S. Iakovlev, J.F. Sigrist, A fully elastic model for studying submerged circular cylindrical shells subjected to a weak shock wave, *Mecanique & Industries* 10 (2009) 275–284.

[14] S. Iakovlev, Interaction between a submerged evacuated cylindrical shell and a shock wave. Part I: diffraction-radiation analysis, *Journal of Fluids and Structures* 24 (2008) 1077–1097.

[15] M.C. Junger, D. Feit, *Sound, Structures, and their Interaction*, MIT Press, Cambridge, USA, 1972.

[16] S. Iakovlev, Interaction between a submerged evacuated cylindrical shell and a shock wave. Part II: numerical aspects of the solution, *Journal of Fluids and Structures* 24 (2008) 1098–1119.

[17] J.F. Sigrist, C. Leblond, Une methode semi-analytique pour l'analyse de l'interaction entre une onde de choc et une coque elastique immergee. Application au dimensionnement de coques de sous-marins, *Mecanique & Industries* 9 (2008) 543–550.

[18] S. Iakovlev, Interaction between an external shock wave and a cylindrical shell filled with and submerged into different fluids, *Journal of Sound and Vibration* 322 (2009) 401–437.

[19] A.C. Ahyi, P. Pernod, O. Gatti, V. Latard, A. Merlen, H. Uberall, Experimental demonstration of the pseudo-Rayleigh (A_0) wave, *Journal of the Acoustical Society of America* 104 (1998) 2727–2732.

[20] M. Sun, K. Takayama, Conservative smoothing on an adaptive quadrilateral grid, *Journal of Computational Physics* 150 (1999) 143–180.

[21] D. Drikakis, D. Ofengeim, E. Timofeev, P. Voionovich, Computation of non-stationary shock-wave/cylinder interaction using adaptive-grid methods, *Journal of Fluids and Structures* 11 (1997) 665–691.

[22] S. Iakovlev, Inverse Laplace transforms encountered in hyperbolic problems of non-stationary fluid–structure interaction, *Canadian Mathematical Bulletin* 50 (2007) 547–566.

[23] M. Abramowitz, I.A. Stegun, *Handbook of Mathematical Functions*, Dover Publications, 1965.